Volume 10
Number 33
7 September 2022
Pages 11815–12144

Journal of Materials Chemistry C

Materials for optical, magnetic and electronic devices

rsc.li/materials-c

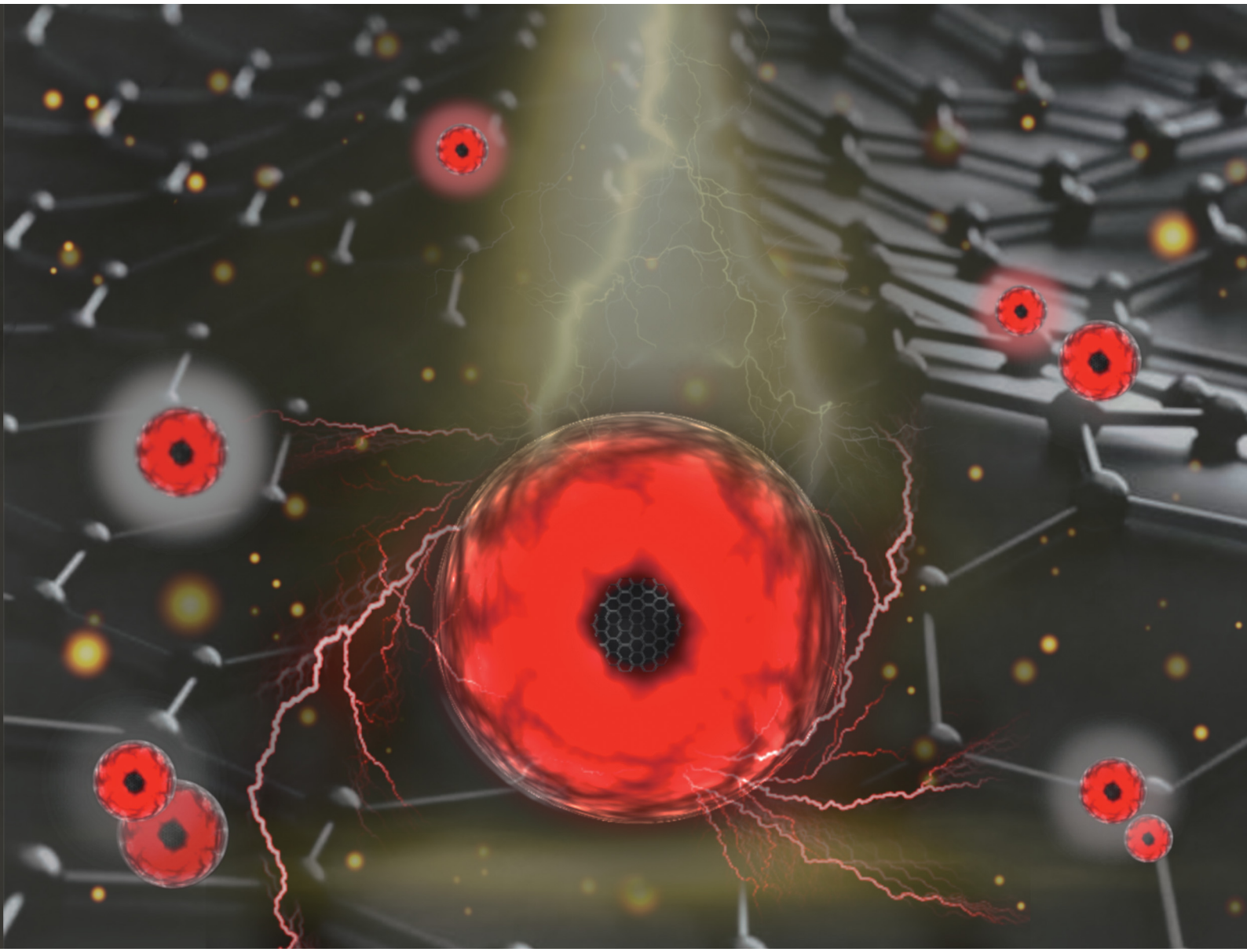

ISSN 2050-7526

ROYAL SOCIETY OF CHEMISTRY

REVIEW ARTICLE

Elisa Moretti, Haiguang Zhao, Alberto Vomiero *et al.*
Synthesis, optical properties and applications of red/near-infrared carbon dots

Journal of Materials Chemistry C

ROYAL SOCIETY OF CHEMISTRY

REVIEW

View Article Online
View Journal | View Issue

Cite this: J. Mater. Chem. C, 2022, 10, 11827

Synthesis, optical properties and applications of red/near-infrared carbon dots

Yi Han,[a] Letizia Liccardo,[b] Elisa Moretti,*[b] Haiguang Zhao*[a] and Alberto Vomiero*[bc]

Compared to inorganic quantum dots, fluorescent carbon nanomaterials (C-dots) have gained significant attention because of their unique optoelectrical properties and low toxicity. Although many review articles summarized the last research achievements, only a few of them are focusing on red/near-infrared C-dots. Due to their unique optical and optoelectrical properties in the red/near-infrared region, this interesting subclass of C-dots may be applied as important building blocks for several applications spanning from bioimaging and nano-thermometry, to luminescent solar concentrators (LSCs) and photoelectrochemical systems. Therefore, in this review the synthesis and the fluorescence mechanism together with the most important applications in thermometry, bio-imaging, LSCs and photocatalysis of red/near-infrared C-dots are considered. Furthermore, another aim is to highlight the available approaches to improve the carbonization degree and, additionally, to discuss the structure/composition correlated optical properties. Finally, outlooks, future perspectives and challenges are also discussed for these highly promising nanostructures.

Received 18th May 2022,
Accepted 21st July 2022

DOI: 10.1039/d2tc02044k

rsc.li/materials-c

1. Introduction

According to the accepted definition, semiconductor quantum dots (QDs) are semiconducting nanocrystals with a typical size below 20 nm, which exhibit semiconducting behavior and optoelectronic properties influenced by the quantum confinement of charge carriers.[1] Thanks to quantum confinement, their optical and electrical properties can be well-controlled by tuning their size and shape.[2–6] Due to their excellent optoelectrical properties, they have been widely used in various applications, including solar cells, light emitting diodes (LEDs), and luminescent solar concentrators (LSCs), in the field of biosensors and bio-imaging, and, finally, as photocatalysts.[2–9] During the last two decades, many types of QDs have been successfully designed and produced using different approaches, including physical and chemical methods.[2–6] Typically, inorganic QDs are composed of metal elements, such as Pb, Cd, In, and Ag, which are either toxic or contain non-earth-abundant rare metals.[2–6,10,11] However, for future applications and commercial purposes, it is preferable and useful to produce low-cost, low toxicity QDs composed of easily available elements.

Compared with various types of semiconductor QDs, carbon dots (C-dots) have attracted much attention because of their metal-free composition (mainly containing C, N and O), low cost and ease of synthesis, using cheap and sustainable precursors.[12–26] C-Dots exhibit broad absorption, bright photoluminescence (PL), and good thermal-, photo- and colloidal-stability.[27–36] Many methods (top-down and bottom-up) have been used to produce C-dots using various types of raw materials.[27–36] They can be produced in a large scale and with a high reaction yield under atmospheric conditions.[27–35] Thanks to the above-mentioned properties, C-dots have been widely used as building blocks for the design of new types of solar cells, catalysts, LSCs, LEDs and bio-applications, such as deep-tissue imaging, biosensing, nanothermometry, and biomedicine (see Scheme 1).[18,20,22–25,27–30,32,33,36–91]

C-Dots were first reported and recognized as a new class of luminescent nanomaterials in 2004 by Scrivens and co-workers.[12] In 2006, Sun and co-workers synthesized luminescent carbon nanoparticles, which are called "carbon quantum dots" (CQDs).[92] Generally, most of the C-dots have a zero-dimensional structure, with a typical size below 10 nm, consisting of a sp^2/sp^3 carbon skeleton and abundant functional groups/polymer chains.[12,14,92,93] The core consists of sp^2/sp^3 carbon atoms, having the graphite/diamond lattice or amorphous carbon form, attributed to the different carbonization degrees.[12,14,92,93] Typically, C-dots are primarily classified into

[a] School of Basic Medicine, State Key Laboratory of Bio-Fibers and Eco-Textiles & College of Textiles and Clothes, Qingdao University, No. 308 Ningxia Road, Qingdao 266071, P. R. China. E-mail: hgzhao@qdu.edu.cn
[b] Department of Molecular Science and Nanosystems, Ca' Foscari University of Venice, Via Torino 155, 30172 Venezia Mestre, Italy. E-mail: elisa.moretti@unive.it
[c] Division of Materials Science, Department of Engineering Sciences and Mathematics, Luleå University of Technology, 971 87 Luleå, Sweden. E-mail: alberto.vomiero@ltu.se

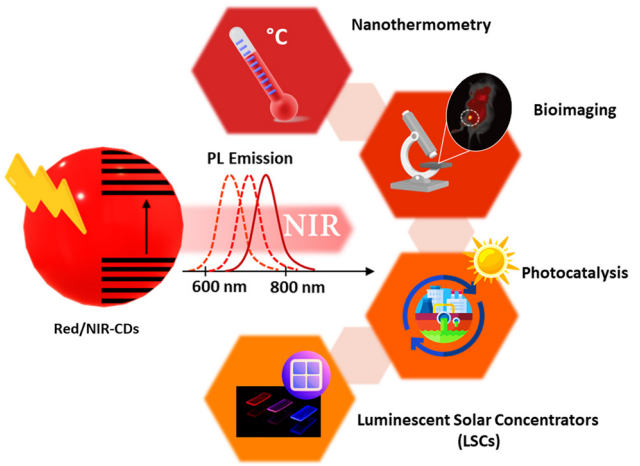

Scheme 1 Examples of the main fields of application of red/NIR C-dots based on their optoelectronic properties, which make them optically active in the red/NIR spectral region.

crystalline graphene QDs, crystalline CQDs and amorphous carbon nanodots (CNDs) depending on their chemical composition and optical properties.[23,36,41,44,94,95] Graphene QDs are composed of a few layers of graphene sheets with lateral dimensions of less than 10 nm.[95] CQDs are composed of multiple layers of graphitic sheets and possess a spherical crystalline structure.[36] Amorphous CNDs are a type of carbon nanoparticle, and usually show a molecular-like structure.[96,97] Beyond this, polymer dots may possess a crystalline structure and an amorphous structure.[26,98–100] Their optical properties may depend on both their core structure and surface functional groups (FGs). In this review article, we mainly focus on crystalline C-dots.

The optoelectronic properties of C-dots can be finely tuned by adjusting their absorption/emission features, and C-dots covering the full range of UV-vis and red/near-infrared (NIR) light were successfully prepared. Compared to UV, blue, green and yellow emitting C-dots, red/NIR emitting C-dots have attracted a lot of attention due to their unique properties, such as deep-tissue penetration, long PL lifetime (compared to the autofluorescence of biological tissues), low levels of photon scattering, and wide absorption, which can be fruitfully exploited in all the applications involving the absorption of solar radiation (see Scheme 1).[18,37,53,77,82–86,101–110]

Although many review articles have summarized the most recent synthesis methods to obtain different types of C-dots with excellent optical properties, and their use in bio-application and energy conversion, there are still a small number of reviews focusing on red/NIR colloidal C-dots and their applications in different fields.[19,20,22,23,25,26,29,30,40,42,47,52,53,58,59,66,72,73,75,84,110–125] Here, we aim to provide a comprehensive overview of the synthesis, the fluorescence mechanism and, finally, the applications of red/NIR crystalline C-dots. In the following sections, we will provide a comprehensive review of the synthesis and optical properties (Section 2), exciton dynamics (Sections 3), and applications (Section 4) of red/NIR C-dots. Finally, we will conclude the current development and future challenges of red/NIR C-dots in Section 5.

2. Synthesis and optical properties of red/near-infrared C-dots

Several methods have been used to synthesize crystalline C-dots, such as hydrothermal, solvothermal, microwave-assisted, self-exothermic reaction and pyrolysis methods,[19,50,90,126–134] which are very easy and do not require an air-free reaction system.[19,50,90,126–134] In addition, most of the synthetic routes for C-dots involved the use of cost-effective and earth-abundant precursors.[68,82,111,133] Hence, this section will focus on the synthesis and the related optical properties of red/NIR crystalline C-dots.

2.1 Citric acid (CA) based precursors

Compared to pyrolysis and hydrothermal approaches, solvothermal and microwave-assisted methods have been widely used for the production of high-quality C-dots. Typically, it is very important to control the carbonization of C-dots by tuning various synthetic conditions, such as the reaction temperature, the use of different precursors and solvents. Up to now, the CA–urea system is one of the most widely used systems for the C-dots production. Both types of precursors (CA and urea) contain earth-abundant elements such as C/O and C/O/N, respectively. Furthermore, they can be obtained at a low cost.[36,120,134] Holá *et al.* reported a hydrothermal route to prepare C-dots from CA and urea in formamide with fluorescence emission in the blue, green, yellow, and red spectral regions.[134] In the same paper, based on transmission electron microscopy (TEM), it is shown that, despite the presence of C-dots exhibiting different colours, they do not exhibit significant size variations (Fig. 1a–d). Moreover, single C-dots exhibit a lattice spacing of 0.22 nm typical of (100) graphitic carbon (the inset of Fig. 1b and d), confirming that different colourations are not derived from the physical sizes of the particles, related to quantum confinement.[134] Instead, the authors demonstrated that the red fluorescence in red C-dots was caused by the increased amount of graphitic nitrogen in the C-dot structure.[134]

Some studies present the size-dependent optical properties.[17,135] The emission peak can be tuned by controlling the sizes of the C-dots.[17,135] For example, Yuan *et al.* reported the synthesis of triangular highly crystalline C-dots by solvothermal treatment or refluxing of precursors in various common solvents. The as-prepared C-dots exhibited different colours by simply varying the size of the C-dots from 1.9 nm to 2.4, 3.0, and 3.9 nm, for blue, green, yellow, and red coloured C-dots, respectively, due to the quantum confinement effect.[135] The optical properties of some C-dots have size-independent optical properties or depend on not only the size, but also the structure and the surface functional groups.[33–36,59] For example, Miao *et al.* reported the synthesis of C-dots with an emission ranging from 550 to 700 nm by controlling both the graphitization and the functionalization

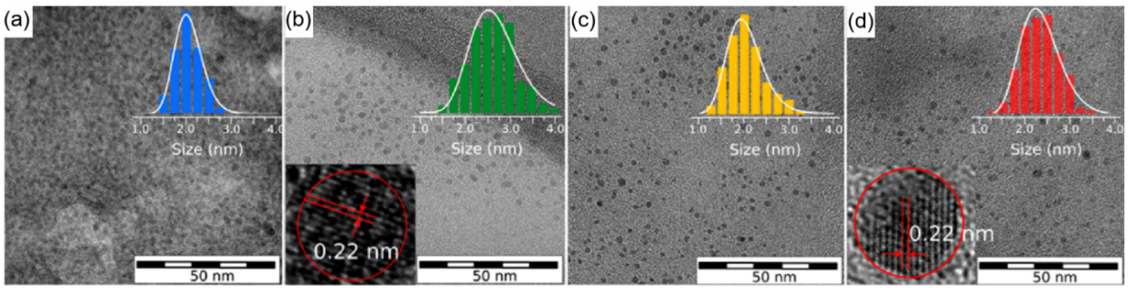

Fig. 1 TEM images of the separated fractions of C-dots with different colours: (a) blue, (b) green, (c) yellow, and (d) red, with diameter histogram and high resolution-TEM images of green and red C-dots in the inset. Reproduced with permission from ref. 134. Copyright 2017, American Chemical Society.

of the C-dots *via* an easy solvothermal method, using dimethylformamide (DMF) as the solvent.[120] As shown in Fig. 2a, these C-dots have a broad absorption and emission when the temperature reaches 200 °C during the synthesis and the molar ratio of CA/urea is over 0.75. The typical quantum yield (QY) of the as-synthesized C-dots is 12.9%, which is much lower than those of green and blue C-dots.[120] The high temperature and high molar ratio of CA/urea contribute to the high carbonization of C-dots, leading to their red emission.[134] Shen *et al.* also synthesized red C-dots employing CA and urea as precursors, but through the use of *N*,*N*-diethylformamide (DEF), instead of DMF, as the solvent. With a lower reaction temperature (160 °C) and a low molar ratio of CA/urea (0.16), the synthesis can produce red C-dots (Fig. 2d).[107] Compared to DMF, DEF can intensify the dehydration reaction between CA and intra-molecules with an ethyl group from DEF and increase the conjugation degree of C-dots.[107] Besides the CA–urea system, CA and ethylenediamine were also used for the synthesis of C-dots with an emission at 550–700 nm and a high QY of 53% (Fig. 2e and f).[76] The red colour and high QY of the C-dots may be obtained from a relatively high nitrogen content (30%) and a high graphitization degree in comparison with other reported C-dots.[76]

2.2 Aromatic compound-based precursors

To improve the graphitization/carbonization degree of C-dots, aromatic compound-based precursors were used for their production.[23,40,44,94,135] Some oxidative or dehydrating agents such as *tert*-butyl hydroperoxide ($(CH_3)_3COOH$), potassium periodate (KIO_4) and concentrated sulfuric acid (H_2SO_4) were also used in the synthesis of red C-dots.[23,40,44,94,135] Wang *et al.* proposed the synthesis of red/NIR C-dots by innovating a sequential dehydrative condensation and dehydrogenative planarization approach at the strong oxidation of KIO_4 using 1,3-dihydroxynaphthalene as the precursor in ethanol solution.[23] As shown in Fig. 2b and c, the as-produced C-dots exhibit an obvious excitonic absorption band located at ~530 nm and an emission peak centered at 628 nm. In addition, C-dots exhibited an excitation independent photoluminescence (PL) behaviour (Fig. 2c). The as-prepared C-dots are large sized conjugated sp^2 clusters with pendent -OH groups at the edge sites. Additionally, they have a QY of 53%.[23] A similar approach was used to produce C-dots using phloroglucinol or 1,3,5-trihydroxybenzene (PG) as the precursor in ethanol or DMF with the presence of dehydrating agents such as concentrated H_2SO_4 or hydrochloric acid (HCl).[135] These C-dots have a well-defined crystalline structure with tunable absorption and emissions (Fig. 2g, h and k). The red C-dots have a PL emission centered at 580 nm with a QY of 53%. Jia *et al.* reported the synthesis of three different red-emissive C-dots passivated with electron-donating groups using *N*,*N*-dimethyl-, *N*,*N*-diethyl-, and *N*,*N*-dipropyl-paraphenylenediamine (NMe_2, NEt_2-, and NPr_2-*p*-PD) in DMF.[34] As shown in Fig. 2I and j, the as-prepared passivated C-dots have emissions centered at 637, 642, and 645 nm, respectively, with a broad absorption ranging from 350 to 650 nm and a high QY of 86.0% in ethanol.[40] Liu *et al.* used conjugated aromatic amine (specifically, tris-(4-aminophenyl)amine) as the precursor and *tert*-butyl hydroperoxide as the oxidative radical reagent for the synthesis of C-dots.[90] These C-dots exhibit a maximum emission wavelength of 615 nm and a very narrow peak width of 26 nm. The absorption spectrum showed a broad absorption with a first excitonic absorption peak centered at 592 nm and a QY of 80.8%.[90]

Recently, the solid-state reaction has been used for the production of high-quality red C-dots.[136–140] Liu *et al.* reported the red/NIR emissive C-dots prepared *via* a solvent-free carbonization approach with a QY of 57%.[136] Zhang *et al.* proposed a solvent-free solid-state method for red C-dot (R-CD) synthesis by utilizing the dehydration self-carbonation effect of the HSO_3 group in 3,4-diaminobenzenesulfonic acid.[137] The as-synthesized R-CDs exhibit a QY of 59% and an emission wavelength in the range of 600–800 nm. Niu *et al.* synthesized red emissive C-dots using phloroglucinol and boric acid as precursors by a solid-state reaction with a yield of up to 75%.[138] These C-dots have the emission ranging from 550 to 800 nm with a QY of 18% with an optimized boron content.[138] Benefitting of the solvent-free reaction, the diffusion of the precursors during the reaction is quite limited, which gives the advantage of the special confined reaction, leading to a uniform size distribution and good optical properties. However, it is still a challenge to mix the precursors uniformly at a molecular scale for large-scale synthesis without using solvents.

2.3 Other precursors

Besides the CA and aromatic compound-based precursors, many other types of precursors have been used to produce

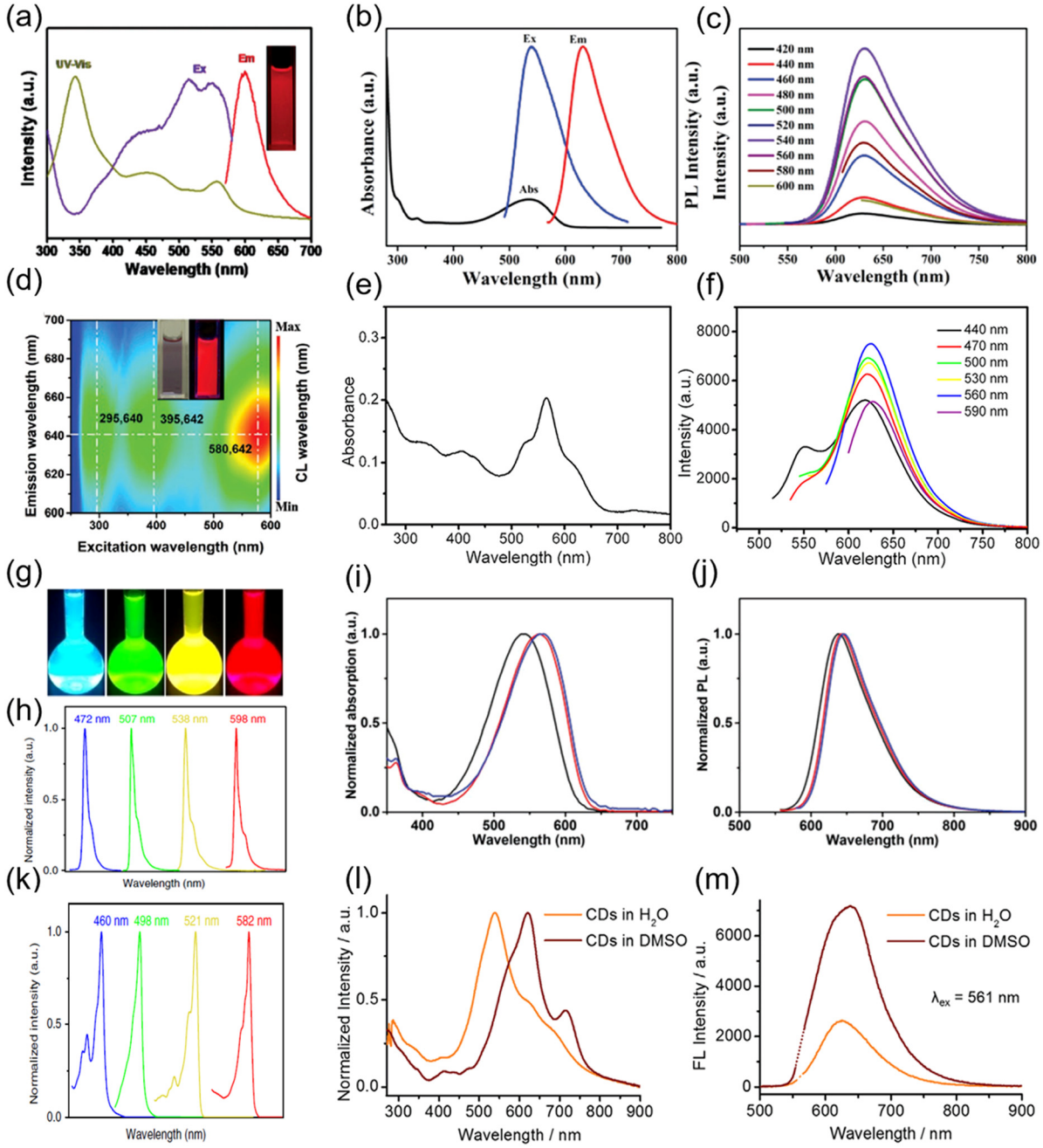

Fig. 2 (a) UV-vis absorption, PL excitation and emission spectra of the red C-dots synthesized using CA and urea as precursors and DMF as the solvent. Inset: The PL image of the C-dots under UV light. Reproduced with permission from ref. 120. Copyright 2018, WILEY-VCH. (b) UV-vis absorption (black), PL excitation (blue), and emission (red) spectra of R-CQDs. (c) PL spectra of R-CQDs excited at different wavelengths. The C-dots were synthesized using 1,3-dihydroxynaphthalene as the precursor and KIO_4 as the oxidation agent. Figure b and c are reproduced with permission from ref. 23. Copyright 2017, WILEY-VCH. (d) PL mapping of the C-dots in the aqueous solution. Inset: The PL image of the C-dots under sunlight (left) and UV light (right). The C-dots were synthesized using CA and urea as precursors and DEF the as solvent. Reproduced with permission from ref. 107. Copyright 2020, WILEY-VCH. (e) UV-vis absorption spectra of C-dots synthesized using CA and ethylenediamine as precursors and formamide as the solvent. (f) Emission spectra of C-dots excited by different wavelengths of light. Figure e and f are reproduced with permission from ref. 76. Copyright 2017, American Chemical Society. (g) Photographs of the C-dots dispersed in ethanol solution under UV light. The emission (h) and absorption (k) spectra of C-dots with different colours. The C-dots were synthesized using phloroglucinol as the precursor. Figure g–k are reproduced with permission from ref. 135. Copyright 2018, Springer Nature. UV-vis absorption (i) and emission (j) spectra of C-dots synthesized using NMe_2-, NEt_2-, and NPr_2-*p*-PD as precursors. Figure i and j are reproduced with permission from ref. 40. Copyright 2019, WILEY-VCH. Absorption (l) and emission (m) of C-dots in water and DMSO. The C-dots were synthesized using CA and urea as precursors and the as-prepared C-dots were further modified with DMSO. Figure l and m are reproduced with permission from ref. 103. Copyright 2018, WILEY-VCH.

high quality C-dots including polymers, dyes, glucose, coal, and biomass (*e.g.* glucose, lignin, fruits, vegetables, and leaves).[139–146] Ye reported the red C-dots using coal as the precursor, with a QY of 0.4% to 1.1%.[140] Ran used a thermal-assisted electrochemical method to produce C-dots using coal slice as the precursor.[141] The as-produced C-dots have a QY of 3%.[141] Obviously, the C-dots synthesized using coal as precursors have low QYs compared to the above-mentioned approaches.[101] As earth-abundant and low-cost resources, biomass has been widely used for the synthesis of C-dots with tunable colours.[142,143] Liu *et al.* reported the preparation of C-dots made from mulberry leaves.[143] The as-prepared CDs have a main emission peak at 676 nm with a shoulder at 725 nm, possessing a full width at half maximum of 20 nm and a QY of 73%.[143] Chen *et al.* reported the synthesis of red emitting C-dots by a solvothermal method using gallic acid, which is a naturally derived polyphenolic compound with a benzene ring.[142] The as-synthesized C-dots showed a fluorescence peak at 585 nm, and a QY of 23%.[142] The main issue for using biomass as precursors to produce C-dots is that the reproducibility of the reaction, as the resources of the biomass, may affect their composition.

2.4 Post-treatment for C-dots

To further obtain the NIR emission, Li *et al.* exploited surface-engineering of the as-prepared C-dots through the electron–acceptor groups (molecules or polymers rich in sulfoxide/carbonyl groups).[103] In detail, the C-dots were first synthesized using CA–urea and then they were treated with dimethyl sulfoxide (DMSO), DMF or *N*-methylpyrrolidone (NMP) solutions by directly redispersing the C-dot powder in the corresponding solvents.[103] As shown in Fig. 2i, the major absorption band of the C-dots dispersed in water appears at 540 nm with a long tail extending into the NIR region (Fig. 2l). After the surface treatment in DMSO, the C-dots exhibit a red-shifted absorption at 619 nm. No significant variation for the emission peak position was recorded after the DMSO treatment (Fig. 2m). However, the QY increases and reached 26% compared to the 6% QY for the untreated sample. In addition, by fixing the excitation wavelength at 732 nm, the DMSO treated C-dots exhibit the NIR emission at 760 nm with a QY of 10%, which represents an efficient candidate for deep-tissue imaging.[103] Recently, Na^+ and Ca^{2+} were also used to modify the surface structure of the visible C-dots.[34,101,120,144] Owing to the improved surface passivation, these metal cations can form a compact cage, which protects the C-dots from the surrounding environment. Zhang *et al.* reported the high QY red C-dots by using the post-treatment approach.[145] After a polyethylene glycol (PEG) post-treatment, the QY increases from 34.2% to 65.5% by improving the surface passivation. As a matter of fact, the C-dot surface treatment using different materials may be a promising approach to obtain red/NIR C-dots. Hence, in Table 1, we summarize the most important synthesis methods using different precursors, and include the details of the optical properties of the as-produced red/NIR C-dots.

Although there are many examples of red C-dots with good water-solubility and bright emission, it is still a challenge to obtain an emission in the second bio-window (700–1100 nm),

Table 1 Comparisons of the synthesis, optical properties and potential applications of the representative C-dots synthesized using different kinds of precursors

Precursors	Solvents	Methods	Abs (nm)	PL (nm)	QY (%)	Application	Refs
CA/urea	DMF	Solvothermal	300–650	570–700	12.9	LED	120
CA/urea	DEF	Solvothermal	300–700	600–700	—	Bioimaging	107
CA/urea (DMSO treated)	DMF	Solvothermal	300–900	550–800	26	Deep-tissue imaging	103
CA/ethylenediamine	Formamide	Solvothermal	300–800	500–750	53	Bioimaging	76
3,4,9,10-Tetranitroperylene (NaOH treated)	NaOH–ethanol	Solvothermal	300–600	550–750	80	LED	39
CA/diaminonaphthalene	Concentrated sulfuric acid	Solvothermal	300–600	500–800	53	LED	25
Dihydroxynaphthalene (KIO_4)[a]	Ethanol	Solvothermal	300–600	550–750	53	LED	23
Tris(4-aminophenyl)amine (*tert*-butyl hydroperoxide)[a]	Ethanol	Solvothermal	200–700	570–700	80.77	Bioimaging	90
Phloroglucinol (H_2SO_4)[a]	DMF/ethanol	Solvothermal/refluxing	300–600	600–700	54	LED	135
NMe_2-, NEt_2-, and NPr_2-*p*-PD	DMF/ethanol	Solvothermal	300–650	600–800	86	LED	40
O-Phenylenediamine/$AlCl_3$	Solvent-free	Solid-state	400–700	550–900	57	Bioimaging	136
Phloroglucinol/H_3BO_3	Solvent-free	Solid-state	200–800	550–800	18	Fingerprint identification	138
Diaminobenzenesulfonic acid	Solvent-free	Solid-state	200–600	600–800	59	Biophotonic	137
Phthalic anhydride and ethylene diamine	Solvent-free	Self-exothermic reaction	200–450	450–650	—	Encrypted ink	132
CA/Tris[b]	Formamide	Solvothermal	300–600	550–750	65.5	Laser	145
P-Phenylenediamine/8-hydroxyquinoline	$ZnCl_2$/tetraethylene glycol solution	Pyrolysis	300–600	500–800	32	Therapy	146
O-Phenylenediamine/ninhydrin	Water	Hydrothermal	300–550	550–800	5–33	LED	147
P-Phenylenediamine/asparagine	Water	Hydrothermal	200–600	400–700	19	LED	152
Phenylenediamine	Water	Microwave	300–500	500–700	8	Bioimaging	153
Mulberry leaves	Ethanol	Solvothermal	200–700	650–800	73	Fluorescent textile	143

[a] The chemicals in the basket are oxidative agents or dehydrants. [b] Polyethylene glycol was used as the surface post-treated agent.

and the absorption onset is below 650 nm. In addition, except for the CA precursor, the precursors used for the C-dot synthesis are not environmentally friendly, and they typically contain relatively toxic chemicals. Additionally, some of them are not stable: this is the case, for instance, of NMe_2, -NEt_2, and NPr_2-PD. Although high QYs have been achieved by using aromatic compound-based precursors, the QY for the majority of the C-dots produced by the CA precursor is still low (less than 20%). Further improvement in the quality of C-dots may focus on the enhancement of the carbonation degree by using the solid-state reaction or pyrolysis reaction,[134–140] and the passivated surface method through post-treatment.[145] Compared to the hydrothermal reaction[147,148] and solvothermal reaction,[103,107,120] the solid-state reaction and microwave-assisted reaction may present more advantages regarding the ease of synthesis and environmental friendless during the large-scale C-dot production.[138,149,150]

3. Exciton dynamics of red/NIR C-dots

The exciton dynamics of the C-dots not only plays a significant role in determining the absorption and emission processes in C-dots, but also provides an effective tool to guide the controllable tuning of the optical properties of C-dots. Typically, several types of PL mechanisms have been reported, including the conjugated π-domain with the quantum confinement effect, surface state luminescence originating from the interaction between the carbon core and surface functional groups, and molecular state luminescence, and aggregation-induced emission (AIE).[59] As shown in Fig. 3a and b, the exciton dynamics might be mainly determined by the core size/composition, the presence of dopants and surface functional groups.[23,25,40–42,44,45,89,94,113,135,150–153] As discussed before, one way to obtain red/NIR C-dots is to improve the carbonization of the C-dots themselves,[135] which can contribute to the creation of highly crystalline C-dots wihtout surface defects, leading to a band-gap emission (Fig. 3a and b, left). For example, Fan *et al.* reported highly crystalline C-dots with multicolor emission.[135] Transient absorption spectra (TA) can be applied to investigate the exciton dynamics in C-dots.[135] As shown in Fig. 4a, two negative peaks of the stimulated emission (SE) exist, centered at 466 and 524 nm, respectively. Four distinctive decay components were identified, with carrier lifetimes of 0.54 ps, 31.5 ps, 77 ps, and 7.3 ns. As shown in Fig. 4b, the fitted decay associated difference spectra (DADS) correspond to the ground state bleaching (GSB) and SE, and the relatively weaker positive (red) features from 600 to 710 nm correspond to the excited state absorption (ESA).[135] The strong emission of the C-dots was demonstrated by the higher amplitude of the emissive component than that of the nonradiative decay component (Fig. 4b). These results not only explain the origin of the double emission peaks, but also the high QY in this type of C-dots.[135]

Zhao *et al.* synthesized high-quality C-dots *via* a vacuum-heating approach and performed TA spectroscopy to obtain insight into the decay channels of the as-prepared C-dots.[36] Fig. 4d and e shows $\Delta T/T$ and the map at a low pump fluence (6.5 $\Delta J\ cm^{-2}$). Two main positive bands are centered at about 410 nm and 520 nm. The SE band at 0.2 ps shows already the spectral features observed in the steady state emission. Throughout the 1.6 ns temporal window they observed that the SE band does not loose significant intensity; this is consistent with the high QY and long fluorescence lifetime.[36]

Some C-dots have excitation-dependent PL spectra and others have excitation independent PL behaviours (Fig. 2c and f). As shown in Fig. 4c, the behaviour might be due to the presence of multiple-energy states.[36] By tuning the excitation wavelengths, PL spectra exhibit a red-shift, as the lower energy photon usually recombines through the lowest energy state of C-dots. Besides the energy states, the broad size distribution of the C-dots also contributes to the excitation-

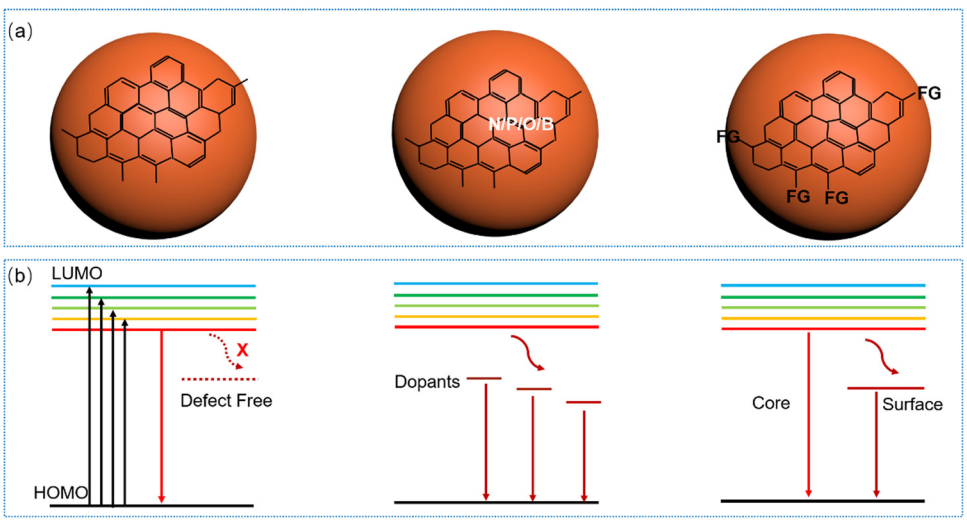

Fig. 3 (a) Structures of various types of C-dots including highly crystalline C-dots (left), doped C-dots (middle) and surface functionalized C-dots (right). (b) Energy band structures of C-dots without surface defects (left), with dopants (middle) and with an intermedium energy level created by the surface functional group (right).

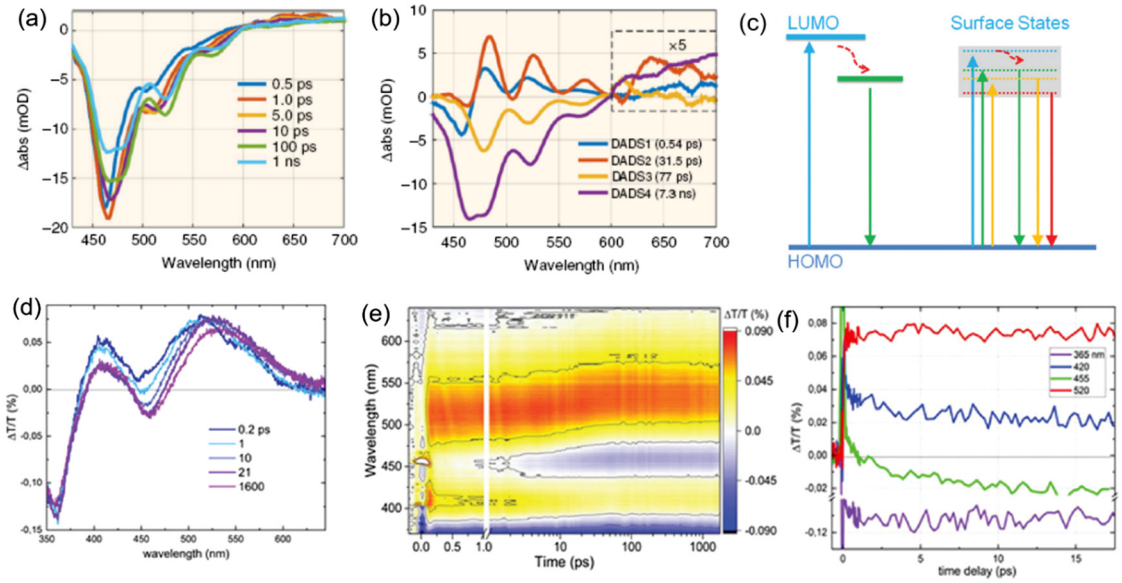

Fig. 4 (a) TA spectra of C-dots at indicated delay times from 0.5 ps to 1 ns. (b) Results of the global fitting with four exponent decay functions. Figure a and b are reproduced with permission from ref. 135. Copyright 2018, Springer Nature. (c) Possible electronic band structure for C-dots produced by space-confined vacuum heating (left) and by the standard solvothermal method (right). Photograph of the TA spectra of C-dots produced by the space-confined vacuum-heating approach: (d) spectra for selected time delays, (e) map, and (f) dynamics for the selected wavelengths; pump@400 nm with a fluence of 6.5 mJ cm^{-2}, pump and probe polarization are set at a magic angle. Figure c–f are reproduced with permission from ref. 36. Copyright 2021, Royal Society of Chemistry.

dependent behaviour in C-dots. For example, by refining a narrow size distribution, the C-dots have an excitation-independent PL spectra.[143] Usually, the highly crystalline core and stable surface functional groups lead to one dominant energy structure (Fig. 4c). For example, the Ca^{2+} cation can bond strongly with the C═O group of C-dots, leading to one dominant energy state.[34] Furthermore, this energy state strongly contributes to the high QY in the C-dots by reducing the non-radiative decay rate. Based on the transient fluorescence lifetime measurement and the following eqn (1) and (2), the radiative and non-radiative decay rates can be directly calculated.[36] Based on these values, the dominant factor affecting the optical properties of the C-dots can be identified, which could guide the optimization of the synthetic conditions for obtaining high-quality C-dots.

$$\tau_{measured} = 1/(k_{rad} + k_{nrad}) \quad (1)$$

$$QY = k_{rad}/(k_{rad} + k_{nrad}) \quad (2)$$

where k_{rad} and k_{nrad} are the radiative and non-radiative decay rates, respectively, and $\tau_{measured}$ is the measured lifetime.

As mentioned before, another way to obtain red/NIR C-dots is to use dopants, which can create intermediate stable energy levels between the band gaps (Fig. 3a and b, middle). Due to the fast decay from the lowest unoccupied molecular orbital (HUMO) energy state to the dopant-related energy state, C-dots only have one dominant PL band.[132,136,154–156] Another possible strategy to obtain red/NIR emissive C-dots is to functionalize their surface through the FG (Fig. 3a and b, right), which could serve as e–h recombination centres, leading to single or double emission. The functionalized C-dots could have surfaces with electron-donating groups (*e.g.* OH, C═O, NH_2), which can increase the highest occupied molecular orbital (HOMO) energy.[109,157] Wu *et al.* utilized hydrophobic C-dots with rotatable surface groups to construct the AIE active glycol C-dot gel.[158] Glycol spontaneously diffused out from the gel layer to allow water intake, which leads to a colour change from the blue dispersion fluorescence to the red AIE.[158] As a summary, the PL mechanism in C-dots originates from many factors. All these factors govern the overall optical properties, leading to complexity in disentangling the PL mechanisms in different C-dots. It was worth to mention that, as the full purification of the C-dots is very difficult,[34] the C-dots were usually decorated by molecular fluorophores. This effect may affect clearly the understanding of the PL mechanism. Although several studies have been carried out, deeper investigations are still required to understand the exciton dynamics of C-dots, especially to have a better idea in the exciton recombination and separation processes, and possible charge transfer, if C-dots are integrated into composite systems. These processes are critically important for the application of C-dots in optoelectronic devices because they affect the efficiency of processes such as light emission, electric power generation and catalytic activity.[123,125] Moreover, they have an influence on most of the optoelectronic properties, such as, for instance, the emission wavelength and the PL lifetime, which are important in nano-thermometry and bioimaging.

4. Applications of red/near-infrared C-dots

4.1 Bio-applications of red/near-infrared C-dots

4.1.1 Toxicity in red/NIR C-dots. In several applications related to living systems, such as theranostics, bioimaging, and

nanothermometry, the assessment of the toxicity of different materials and structures interacting with the living body is mandatory. Although C-dots are considered to be less toxic and more biocompatible, compared to other inorganic QDs (*e.g.* PbS, Ag_2S and CdSe/ZnS), it is still important to investigate accurately their *in vitro* and *in vivo* toxicity.[56,159] The main methodologies to investigate the cytotoxicity of C-dots are the MTT-based assay, Cell Counting Kit-8 (CCK8)-based assay, reactive oxygen species (ROS) generation analysis, flow cytometric analysis and so on.[56,159] Beyond these methods, histopathological examinations, hematoxylin and eosin (H&E) stain images, behavior and weight observation, are also used for *in vivo* toxicity evaluation.[56,159]

MTT is the mostly used method for toxicity evaluation and has also been applied to C-dots. For example, NIR C-dots derived from the lemon juice were evaluated using the MTT assay.[83] After 48 h incubation of NIR-C-dots [with a concentration (C) up to 1000 μg mL^{-1}] for HeLa cells, the cell viability still maintained 90% of its initial value (Fig. 5a). A similar observation was found in 4T1 and HepG2 cells.[37] Xue *et al.* synthesized C-dots using lychee exocarp, chlorin e6 (Ce6) and transferrin.[82] After incubation of free Ce6 with a concentration of 15 μg mL^{-1} for 6 hours, the viability of Bel-7404 cells maintained 81%, whereas the viability of cells incubated with the same concentration of C-dots were over 95%.[82] Hypocrella bambusae was used for the synthesis of C-dots,[160] and the MTT assay indicated that the HeLa cell viability was still high even with a concentration up to 200 μg mL^{-1}. C-Dots were synthesized *via* a one-step microwave method using citrate and L-tryptophan as precursors.[161] Ce6-Loaded assembled C-dots (A-C-dots@Ce6) was prepared *via* the assembly of the negatively charged discrete C-dots to form a vector loaded with the photosensitizer Ce6.[153] The CCK-8 assay showed that the 549 cells retained 90% of its cell viability after incubation for 24 hours with an A-C-dots@Ce6 concentration of 16 μM.[161] Moreover, Liu *et al.* found that the photodegradation of C-dots could cause cytotoxicity through CCK-8.[161]

Cell apoptosis was used to evaluate the toxicity of C-dots. C-Dots prepared from polythiophene and diphenyl di-selenide were introduced for cell apoptosis evaluation, and the viabilities of HeLa cells had no obvious variation between the control and the C-dots (24 h incubation, a concentration of 40 μg mL^{-1}) (Fig. 5b and c).[81] ROS generation is another important indicator of cytotoxicity. The ROS generation of C-dots was evaluated using mesenchymal stromal cells (MSCs) after 45 min incubation.[162] The ROS level was 2.2 times higher than the controlled sample with a C-dot concentration of 200 μg mL^{-1}. A similar trend was found after the C-dots were incubated for 24 h with an identical concentration (Fig. 5d).[156] The increase of the ROS level indicated that C-dots may help the cell starting the antioxidant process.[162]

The toxicity *in vivo* was studied through many methods, such as H&E staining or the behavior/weight observation of mice. The major organs of the mice of the control group and Ce6 modified red C-dot treated group were harvested after injecting the C-dots (100 μL, 1.0 mg mL^{-1}) into mice for 13 days. It was found that there is no obvious variation and damage between two groups (Fig. 5e).[163] In addition, there was no obvious difference of the mice body weight among all groups. These results indicated that the Ce6 modified red C-dots did not show any significant toxicity *in vivo*.[163] To sum up, for toxicity evaluation using different methods, the C-dots

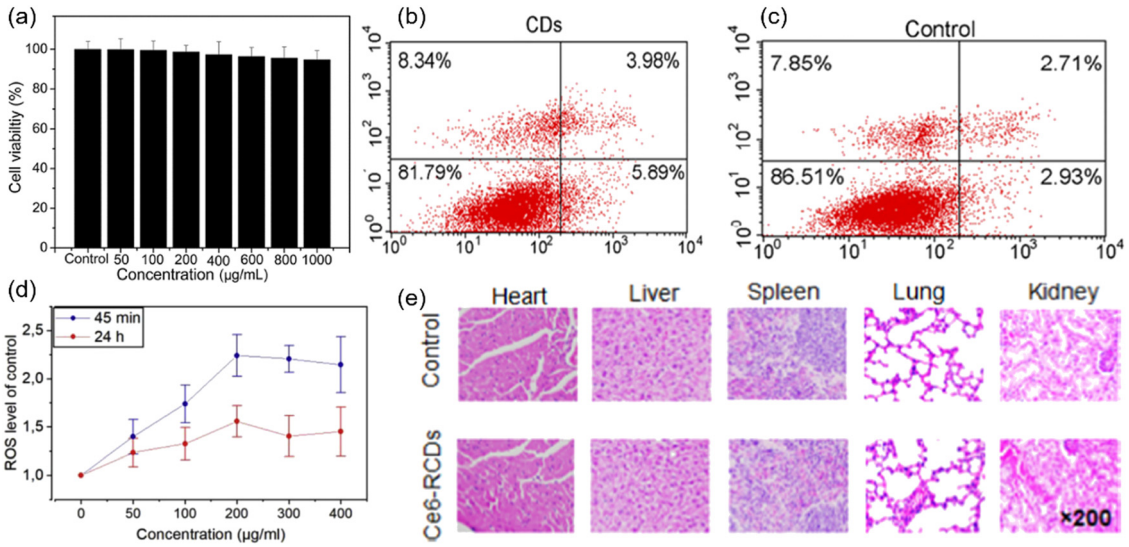

Fig. 5 (a) Cell viability of the C-dots at an increasing concentration from 0 to 1 mg mL^{-1} on HeLa cells using the MTT assay. Reproduced with permission from ref. 83. Copyright 2019, Elsevier Ltd. (b) Flow cytometry analysis of apoptosis and necrosis of HeLa cells incubated with C-dots alone, and (c) control sample without C-dots and laser irradiation. Reproduced with permission from ref. 81. Copyright 2018, American Chemical Society. (d) ROS generation after 24 h incubation with various concentrations. Reproduced with permission from ref. 162. Copyright 2019, Elsevier Ltd. (e) Hematoxylin and eosin (H&E) staining of major organ sections gathered from the control and C-dots treatment groups at 24 h post-injection. Reproduced with permission from ref. 163. Copyright 2019, American Chemical Society.

exhibited low toxicity and biocompatibility at a large range of C-dot concentration levels (up to 1000 μg mL^{-1}). However, very few reports exist about the long term toxicity of C-dots, especially *in vivo*. There is still a lack of deep investigation for the mechanism of cytotoxicity. The interactions between C-dots and biomacromolecules also deserve to be investigated to study the metabolic mechanism of C-dots.

4.1.2 Nanothermometry based on red/NIR C-dots. Considering the excellent optical properties and biocompatibility of the colloidal C-dots, they have been used as a fluorescence non-contact thermometer in living cells for biology and biomedicine process detection. Benefiting from the deep-tissue penetration, red/near infrared C-dot nanothermometers exhibited a great potential for real application compared to UV-vis emitting C-dots.[28–30,32,33,36,46,50,51,53] Different types of nanothermometers have been recently studied, including double emission self-calibrating thermometers and the multi-parametric thermometers based on the simultaneous measurement of different physical/chemical quantities.[164,165]

C-Dots were prepared using Mangifera indica, exhibiting a red colour. The C-dots have a temperature dependent PL spectrum ranging from 10 to 80 °C.[77] The further intracellular PL measurement was carried on in the range of 25–45 °C in live L929 cells. The PL intensity of the C-dots decreased with the increase of the temperature. Another red-emitting C-dots derived from thionine and CA showed a linear relationship between the PL intensity and temperature ranging from 4 to 80 °C, with a thermal sensitivity of ~1.2% $°C^{-1}$. Experiments on MCF-7, HepG2 and A549 cell lines were implemented to testify the intracellular temperature-responsive PL of the C-dots (Fig. 6a).[166] The intracellular red fluorescence emission intensity gradually decreases accompanied by a temperature reduction from 37 °C to 20 °C. The red fluorescence recovered in the heating process back to 37 °C. Wang *et al.* prepared red emissive C-dots to detect glutathione (GSH) in cells.[167] They found that the PL of the C-dots quenched by GSH recovered when the temperature increased, which showed a potential for efficient nanothermometers. The thermal sensitivity of these C-dots for the temperature measurement is approximately 1.07% $°C^{-1}$. This trend of the PL intensity of the as-prepared C-dots is different from that of the other C-dots, when the temperature increases from low to high degrees, the fluorescence intensity of C-dots also increased (Fig. 6b).[166] When the temperature increases from 10 to 80 °C, the fluorescence of C-dots–GSH recovers gradually and the fluorescence intensity increases by 75.0%.[166] Typically, besides the temperature, the optical sensor based on single emission C-dots could be sensitive to other environmental conditions, such as biomolecules, solvents and pH, which are largely affecting the accuracy of the thermal sensor. Up to now, the sensitivity of thermal sensors based on single-emission C-dots is still relatively weak. Compared to the single emission, ratiometric optical nanothermometry relies on the ratio of two PL signals for probing the temperature changes in the surrounding media.[31,168] Ratiometric optical thermometry allows the self-calibration of the system with improved robustness and reliability. Dual emission C-dots were synthesized using precursors of CA and urea.[168] The as-prepared C-dots exhibited two peaks located at 440 nm and 590 nm, respectively. The PL intensity ratio of two channels exhibited a temperature dependence ranging from 15 to 80 °C.[168] Specifically, the PL intensity at 590 nm decreased obviously when the temperature was increasing, while the PL intensity at 440 nm remained unchanged. However, these systems have a serious drawback that the PL does not fall in any water transparency window, so the penetration depth of emitted light is rather limited.

Han *et al.* reported a ratiometric thermal sensor based on hydroxyl functionalized C-dots synthesized *via* a hydrothermal approach using phloroglucinol as the precursor.[31] The C-dots exhibited the dual emission originating from the band gap emission and surface-dominant emission, respectively, which show a different temperature-dependent PL response. The integrated PL area ratio between 566–700 nm and 500–535 nm exhibited linear dependence on the intracellular temperature in the range of 32–42 °C.[31] C-dots@OH was employed to monitor the intracellular temperature (32–42 °C) through

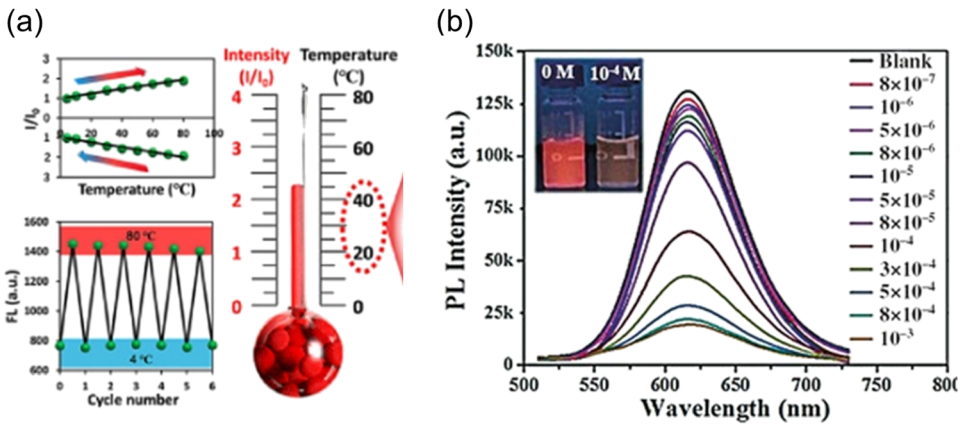

Fig. 6 (a) Red-emitting C-dot wide-range responsive nanothermometers for temperature sensing (4–80 °C). Reproduced with permission from ref. 166. Copyright 2020, American Chemical Society. (b) Fluorescence spectra of red-emitting C-dot solution with GSH (0.1 mm) at different temperature heating up from 10 to 80 °C under an excitation wavelength of 480 nm. Reproduced with permission from ref. 167. Copyright 2016, WILEY-VCH.

confocal fluorescence microscopy with two typical channels, showing a clear trend for the temperature variation in a single cell (HEK 293T). As shown in Fig. 7a–h, a clear red fluorescence from the second channel and green fluorescence from the first channel were clearly observed when they were stimulated using a 488 nm laser.[31] The fluorescence intensity decreased with the increase of temperature from 32 to 42 °C (Fig. 7i). The fluorescence density ratio of $I_{566-700}/I_{500-535}$ was calculated by using the average fluorescence intensity of 10 individual cells, which exhibited linear dependence on temperature in the range of 32–42 °C. The obtained slope is −0.2, indicating that C-dots could be potentially used as the ratiometric thermal sensor in biological systems. In addition, the PL ratio is stable as a function of incubation time (Fig. 7j), indicating that the thermal sensor showed a great potential for the real cell measurement.[169]

Even if C-dots show a potential for use as the nanothermal sensor, it is still a challenge to produce a stable sensor because of the sensitivity of the fluorophores to the surrounding complicated environmental conditions *in vivo*. This drawback could be overcome through the following strategies: (i) design and produce the super-stable fluorophores; (2) coating the C-dots with a robust shell (silica shell or polymer shell) against the side effect from the environment; (3) build up a reliable calibration curve database of the sensor under different conditions (biomolecules, pH and composition of the environment).

4.1.3 Deep-tissue bio-imaging based on red/near infrared C-dots. Bio-imaging is one of the most attractive applications of C-dots. In particular, for red/NIR C-dots, because of their lower emission damage to the tissue and deep tissue penetration, they are widely used for deep-tissue bio-imaging. Three types of effects are introduced for bioimaging, including down-conversion, up-conversion, and photoacoustic (PA) imaging. Down-conversion PL imaging is the most widely used method. Hua *et al.* synthesized red emissive (at ~605 nm) nickel doped C-dots (Ni–C-dots) using *p*-phenylenediamine and nickel ions as raw materials.[170] Tumor-bearing mice were used for imaging performance evaluation through an intratumoral injection of Ni–C-dots. The fluorescence intensity of the tumor region decreased as a function of time. Ni–C-dots accumulated in the tumor sites after 1, 3, and 7 days post-injection. No obvious fluorescence was found in other major organs as shown in Fig. 8a. Wide color gamut PL tunable C-dots were prepared from L-glutamic acid and *o*-phenylenediamine with different

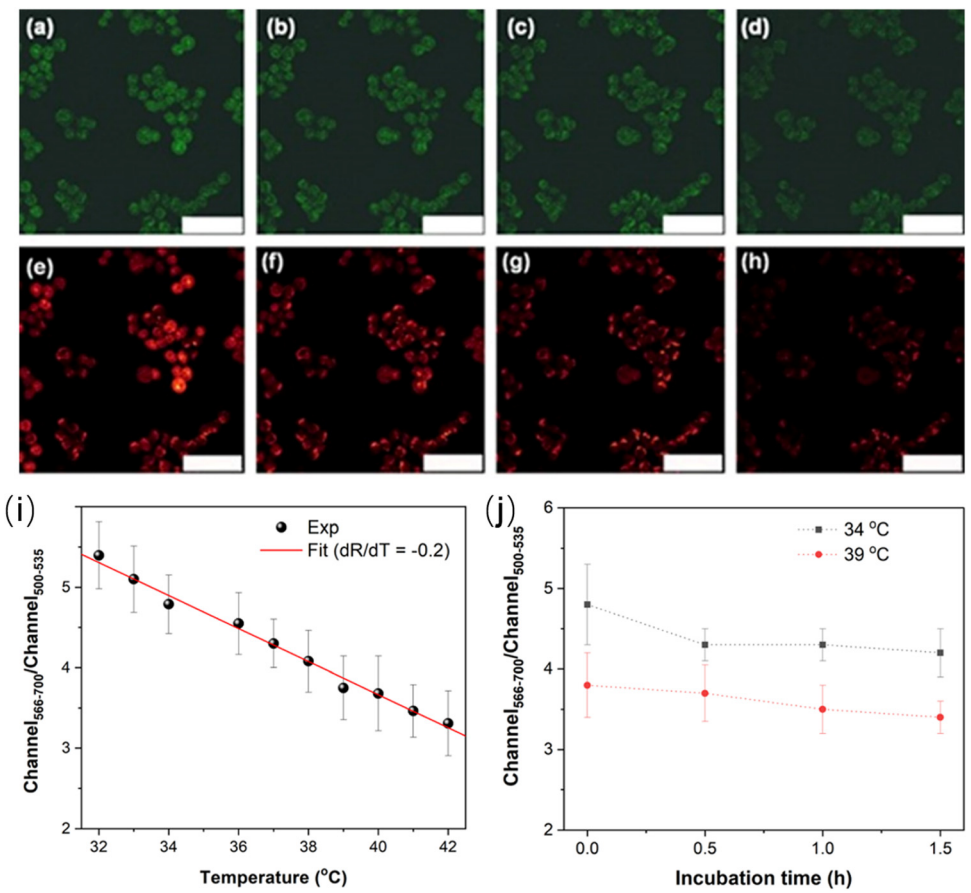

Fig. 7 Microscopy images under different temperatures. (a–d) Images of the first channel (500–535 nm) at (a) 32 °C, (b) 36 °C, (c) 38 °C, and (d) 42 °C, respectively. (e–h) Images of the second channel (566–700 nm) at (e) 32 °C, (f) 36 °C, (g) 38 °C, and (h) 42 °C, respectively. Scale bar is 75 μm. (i) Linear relationship between the ratio of fluorescence intensities of two channels and temperature. (j) Ratiometric response of the fluorescence intensity as a function of incubation time. Reproduced with permission from ref. 31. Copyright 2021, Royal Society of Chemistry.

solvents.[91] The emission of red C-dots located at 713 nm. The PL images of nude mice after subcutaneous injection of the C-dots within 1 h were evaluated under an excitation wavelength of 600 nm. The C-dots could penetrate tissues of mice without a significant decrease of PL. Wen *et al.* synthesized red–NIR-light emitting (680 nm) C-dots using pheophytin powders as the source.[85] After the intravenous injection of C-dots in tumor-bearing mice, PL signal intensities in tumor sites kept increasing for the first 8 h. Even for 24 h, the PL intensity in tumor sites was still higher than other organs (Fig. 8b). Li *et al.* developed novel NIR-emitting C-dots using watermelon juice as the source.[171] The as-prepared C-dots exhibited emissions from 900 to 1200 nm with a peak centered at 925 nm under 808 nm laser excitation. A NIR imaging apparatus was

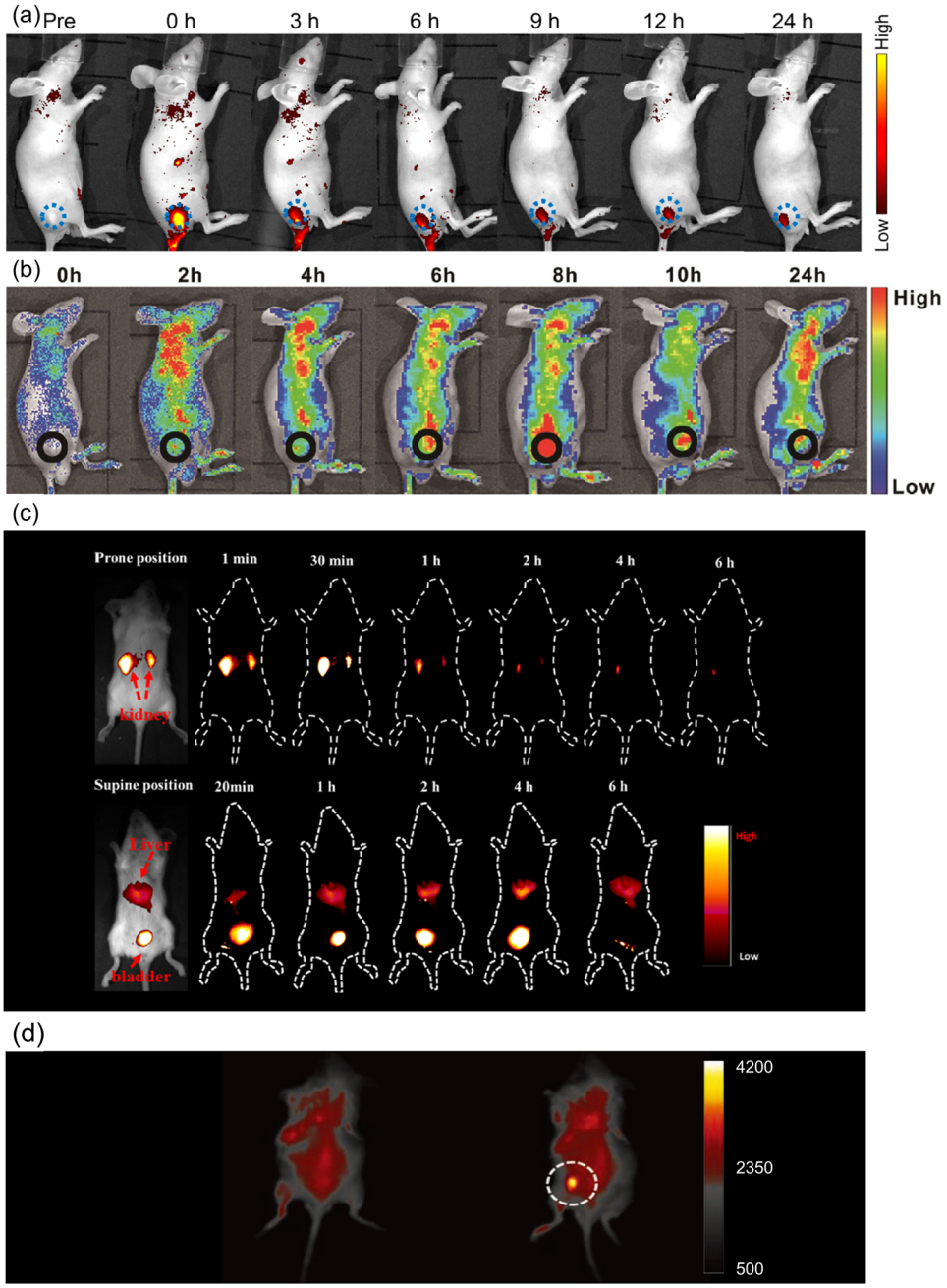

Fig. 8 (a) *In vivo* FL images of mice after intratumoral injection of Ni-pPCDs (dose: 0.5 mg kg^{-1}). Blue dotted circles indicate the tumor areas. Reproduced with permission from ref. 170. Copyright 2019, American Chemical Society. (b) *In vivo* FL images of mice after intravenous injection of C-dot assembly in water. Reproduced with permission from ref. 85. Copyright 2019, WILEY-VCH. (c) *In vivo* FL images of mice treated with C-dots (20 μg g^{-1}) through the tail vein. Reproduced with permission from ref. 171. Copyright 2019, American Chemical Society. (d) *In vivo* NIR up-conversion luminescence images of a mouse before (left) and after (right) the subcutaneous injection of NIR C-dots. Reproduced with permission from ref. 105. Copyright 2019, WILEY-VCH.

used for *in vivo* bioimaging under a 1000–1400 nm band pass filter. After 1 min injection through tail vein of the mice, the PL signal was found in kidneys, and the PL signal became very weak after 6 h, which indicated the rapid excretion of C-dots (Fig. 8c). Zhang *et al.* used the red emissive bovine serum albumin treated C-dots for *in vivo* tumor imaging and two-photon fluorescence imaging of blood vessels in mouse ear.[172]

The up-conversion emitters could emit short-wavelength fluorescence under long-wavelength excitation, which could provide a greater penetration depth of both excitation and emission light and improve the quality of PL imaging. Li *et al.* synthesized up-conversion NIR emitting C-dots by microwave-assisted exfoliation in DMF with the emission peak located at 784 nm under 808 nm laser excitation.[105] After the subcutaneous injection of NIR C-dots, the high PL intensity signal of NIR C-dots was captured on the back of the mouse (Fig. 8d). Except for mice, zebrafish larvae were also used for NIR-II two-photon bio-imaging through red-emitting C-dots. Liu *et al.* prepared highly efficient ultra-narrow red-emitting C-dots using conjugated aromatic amine as the precursor.[90] Zebrafish larva was maintained in diluted C-dot aqueous solution for 2 h. Through the NIR-II excitation, the emission could penetrate ~500 μm of the tissue, which is helpful in reconstructing the three-dimensional (3D) bio-imaging of the Zebrafish larva. There are only a few reports on deep tissue up-conversion bio-imaging using C-dots, but this seems being a highly promising direction.

Photoacoustic (PA) imaging is a new non-invasive bio-imaging method. The C-dots can produce an ultrasonic signal when irradiated by a pulsed laser. PA imaging combines with the advantages of the optical imaging and ultrasound imaging methods, which are helpful to enhance the resolution of the deep tissue bio-imaging through a multiparametric platform. Ge *et al.* prepared red-emissive C-dots using polythiophene phenylpropionic acid (PPA) as the precursor.[118] The HeLa tumor bearing mice were intravenously injected with C-dots, and the PA images of tumor within 24 h were captured. It was found that the C-dots accumulated in the tumor could emit constant PA signals after circulation in blood vessels. Similar results are also found in sulfur and nitrogen co-doped NIR C-dots.[37] Mice with 4T1 tumors were intravenously injected with the NIR C-dots. PA maximum amplitude projection images and B-scan PA images of the tumor within 24 h were recorded. The C-dots accumulated uniformly in the tumor tissue and the intensity of the PA signal reached the highest point at 3 h post-injection. After the intravenous injection of C-dots using *Hypocrella bambusae* as the precursor, a clear tumor microstructure was captured through PA imaging with a high spatial resolution.[160] The signal intensity of tumors indicated the C-dots could accumulate in tumor within 8 h post-injection, which could be regarded as the optimum point for laser irradiation and other therapies. Overall, most current research studies focus on red and NIR-I C-dots for bio-imaging, but the NIR-II channel bioimaging could improve the tissue penetration depth and imaging sensitivity. In addition, it is very important to produce NIR-II emissive C-dots with stable emission. For example, concerning C-dots, any of PL quenching that occurs could affect the accuracy of the thermal sensor. Thus, one should design dual emitters in one C-dots by the bandgap emission and inter-band emission as shown in Fig. 10a.

4.2 Luminescent solar concentrators (LSCs) based on red/near-infrared C-dots

LSCs can be defined as large-area sunlight collectors. They are able to absorb sunlight and emit the radiation at lower energies. Commonly, the emitted light can be waveguided inside the slab until reaching its edges, where it can be converted in electricity by properly attached solar cells (Fig. 9).[28–30,32,33,36,46,50,51,53,173] Typically, the configuration of the LSCs includes the tandem structure, thin film structure and polymer matrix (Fig. 9a–c). Due to their low weight, low-cost and semitransparency, LSCs could be potentially used for building integrated photovoltaics (BIPVs). There are several factors affecting the optical efficiency of the LSCs. Besides the energy loss from unabsorbed light and reflected light from the top surface, the energy could be lost though the (1) absorption/re-emission process, because the QY of the C-dots might be below 100%; (2) part of the emission might be lost due to re-absorption; (3) partial emission falls into the so-called escape cone.[28] For example, in the case of a glass or polymer matrix, with a refractive index of ~1.5, about 75% of the incident radiation can be captured by a LSC waveguide. The reabsorption energy loss plays a dominant role for the power conversion efficiency (PCE) of LSCs, since their sizes can be very large (up to one meter).

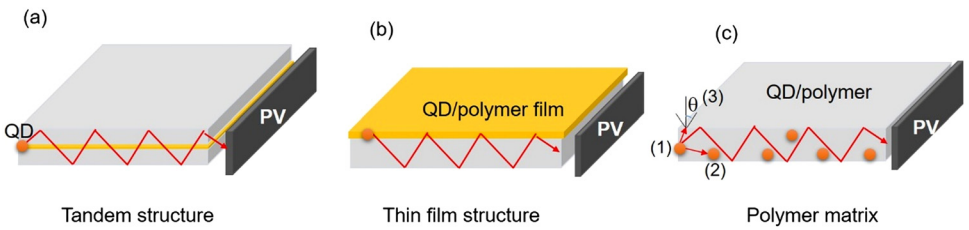

Fig. 9 Schematic representation of a C-dot-based LSC with different configurations: (a) tandem structure; (b) thin film structure and (c) polymer matrix. The numbers indicate the typical processes of energy loss in an LSC. (1) The light was absorbed by the QDs, but there is a partial energy loss because of the non-unity of the QY; (2) emission is reabsorbed by another QD due to the overlap between the absorption and emission spectra. (3) Re-emitted incident light escapes from the surface due to the escape cone.

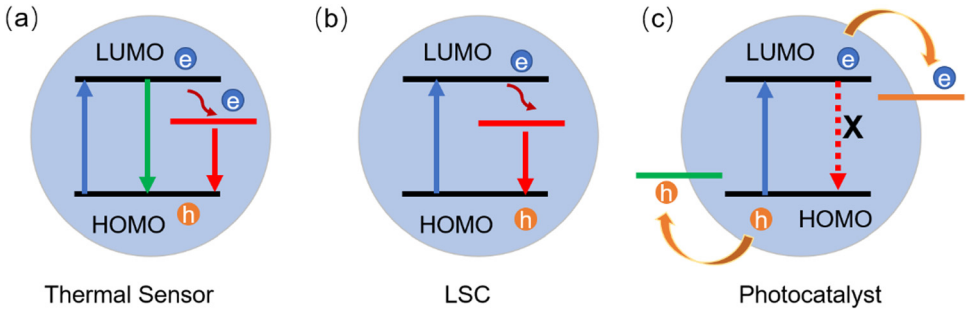

Fig. 10 Energy diagrams of different types of C-dots for the (a) thermal sensor, (b) LSC and (c) photocatalyst.

As shown in Fig. 10b, the intermedium band emission can offer a large Stokes shift (the energy gap between the maximum peak position of the absorption and emission), thus largely reducing the reabsorption energy losses.[36] Nowadays, various types of fluorophores have been used as a sunlight absorber/converter for LSCs, including organic dyes/polymers, quantum dots, perovskites, and C-dots.[36,174] Although the use of C-dots can be beneficial as they are less-toxic and low cost, the synthesis of C-dots with a broad absorption, large Stokes shift, and high QY remains still a great challenge.

Up to now, several groups have reported the use of C-dots for LSC production including single-layer and tandem structures.[28,51] UV-vis emitting C-dots have been used for LSC fabrication.[28,51] For example, Gong's group and Rosei's group have synthesized nitrogen-doped C-dots for LSCs.[11,46] Zhao *et al.* developed an LSC using visible C-dots produced by the vacuum-heating approach.[36] The as-prepared C-dots have a high QY of 65%, a large Stokes shift of 0.53 eV, and a broad absorption range (300–500 nm).[36] The single-layer LSC (15 × 15 × 0.5 cm^3) prepared by using the polyvinyl pyrrolidone (PVP) polymer as a matrix exhibits an external optical efficiency (the power ratio between the power at the edges and surface of the LSC) of 2.2% (under natural sun irradiation, 60 mW cm^{-2}). As red/NIR C-dots can absorb more solar light compared to visible-emitting C-dots, several groups are now focusing on LSCs made with red/NIR C-dots. Wang *et al.* produced LSCs, by synthesizing red (R-) C-dots with a 15% of QY, through a one-step solvothermal process using phenylenediamine isomers in the presence of lignin.[50] As shown in Fig. 11a and c, the LSCs were semitransparent and presented a clear bright colour on the edges upon UV illumination. By tuning the thickness of the C-dot layer, the yellow (Y-) C-dot-based LSC exhibited a ~72% transmittance (Fig. 11b). The R-, Y-, G- (green) C-dot LSCs exhibited wide PL spectra, well matching the Sun's spectrum (Fig. 11d). Fig. 11e presents the typical *J*–*V* characteristic curves of the C-dot-based LSCs. The as-prepared LSC based on R–C-dots only have a PCE of 1.96% (5 × 5 × 0.1 cm^3), and this

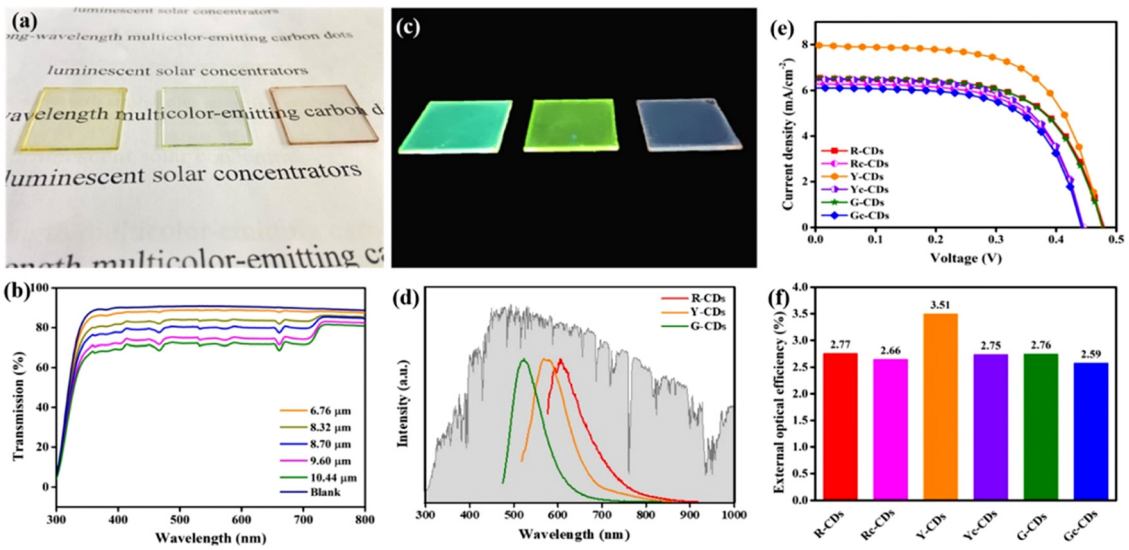

Fig. 11 (a) Photographs of the R, Y, G C-dot-based LSCs under daylight. (b) Transmittance spectra of Y CD-based LSCs with different thicknesses (0.32 wt% of C-dots concentration). (c) Photographs of the R, Y, G C-dot-based LSCs under UV light. (d) Emission spectra of the R, Y, G C-dot-based LSCs. (e) Relationship of the photocurrent density and photovoltage (*J*–*V*) of the various C-dot-based LSCs (0.32 wt% of C-dot concentration, 9.6 μm of thickness). (f) External optical efficiencies of the various C-dot-based LSCs (0.32 wt% of C-dot concentration, 9.60 μm of thickness). Reproduced with permission from ref. 50. Copyright 2020, American Chemical Society.

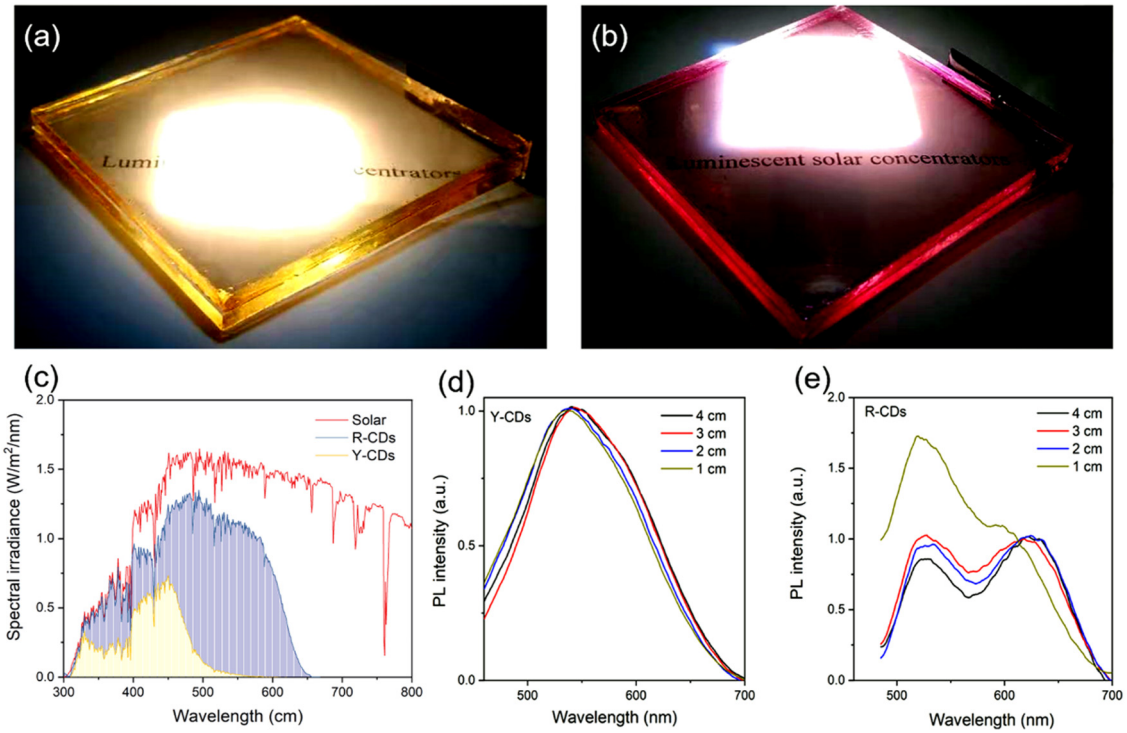

Fig. 12 Photographs of the laminated LSC based on yellow (a) and red C-dots (b) upon one sun illumination. Laminated LSC dimensions, 10 × 10 × 0.9 cm^3. (c) Calculated solar absorption of the LSCs and solar spectrum. The concentration of the C-dots in PVP was 1 wt% in PVP. PL spectra measured at different *L* for the yellow (d) and red C-dot (e) based LSCs. The excitation wavelength is 400 nm. Reproduced with permission from ref. 33. Copyright 2021, Royal Society of Chemistry.

is due to the lower QY of R-C-dots compared to Y- and G-C-dots (Fig. 11f).[50]

Zdražil *et al.* fabricated a tandem LSC composed of three layers using three types of C-dots: blue, green, and red emissive C-dots, respectiveley.[51] The green C-dots were synthesized using 3,4,9,10-tetranitroperylene as the precursor *via* a hydrothermal approach. The red C-dots were further obtained by the conversion of green C-dots adding dropwise a NaOH–ethanol solution. The LSCs were fabricated by deposition of the C-dots–polymer solution onto 8 × 8 cm^2 glass slabs using a drop-casting method. The pictures of the single C-dot-based LSCs under simulated solar light are shown in Fig. 11a–f. All three LSCs appeared highly transparent. Bright concentrated blue, green, and red light were clearly distinguished at the edges of the LSCs upon UV illumination. Compared to blue and green C-dots, the red C-dots exhibited broader absorption, which allows an efficient absorption of solar radiation. Due to the spectral overlap between the absorption and emission spectra, with the increase of the distance (*L*) between the excitation spot and the LSC edge, reabsorption occurs. The tandem LSC (8 × 8 cm^2) based on B, G, and R-C-dots exhibited an optical efficiency of 2.3%.[51] Very recently, Gong's group have used red and yellow emissive C-dots to fabricate a tandem structured LSC by integrating two laminated LSCs. The Y C-dots were prepared *via* phenylenediamine isomers (*o*-PDs) as the precursor *via* a simple hydrothermal approach.[33] The Y C-dots have a QY of 86.4%. The R C-dots were prepared using *o*-PDs and dopamine. The R C-dots have a QY of 17.6%. Compared to the single layer LSC, the laminated structure (C-dots/PVP layers were sandwiched by two slides of glass) can isolate the fluorophores from the surrounding moisture or chemicals, thus providing a promising solution for photovoltaic windows. The as-prepared laminated LSCs based on Y and R CDs are semi-transparent (Fig. 12a and b).[33] The absorption spectrum of the laminated LSC is shown in Fig. 12c. For the R-C-dots, an obvious PL peak shift was found with the increase of *L* from 1 to 2 cm (Fig. 12e), which is due to the spectral overlap between the absorption and emission. In contrast, there is no PL peak shift in the Y-C-dot based LSC (Fig. 12d). The tandem LSC (10 × 10 cm^2) based on Y and R C-dots exhibited a PCE as high as 3.8%.[33]

Cai *et al.* fabricated an LSC based on red emissive C-dots.[175] The C-dots were prepared using bottom-up molecular fusion based on nitrated pyrenes and boric acid. Due to the efficient surface functionalization, the as-prepared C-dots have an excitation-wavelength-independent emission ranging from 550 to 700 nm (Fig. 13a). The C-dots in a polystyrene (PS) matrix have a QY as high as ~90% (Fig. 13b) and a large exciton binding energy (~300 meV), which can strongly resist to thermal quenching.[175] The as-fabricated laminated LSCs (10 × 10 × 0.63 cm^3) exhibited a clear concentrated light at its edges as shown in the inset of Fig. 13c. The *J*–*V* curves of the LSCs are shown in Fig. 3c and d, yielding a PCE of ~1.4%.[175] Summarizing, red/NIR C-dots may represent a viable solution to improve the functionality of LSCs.

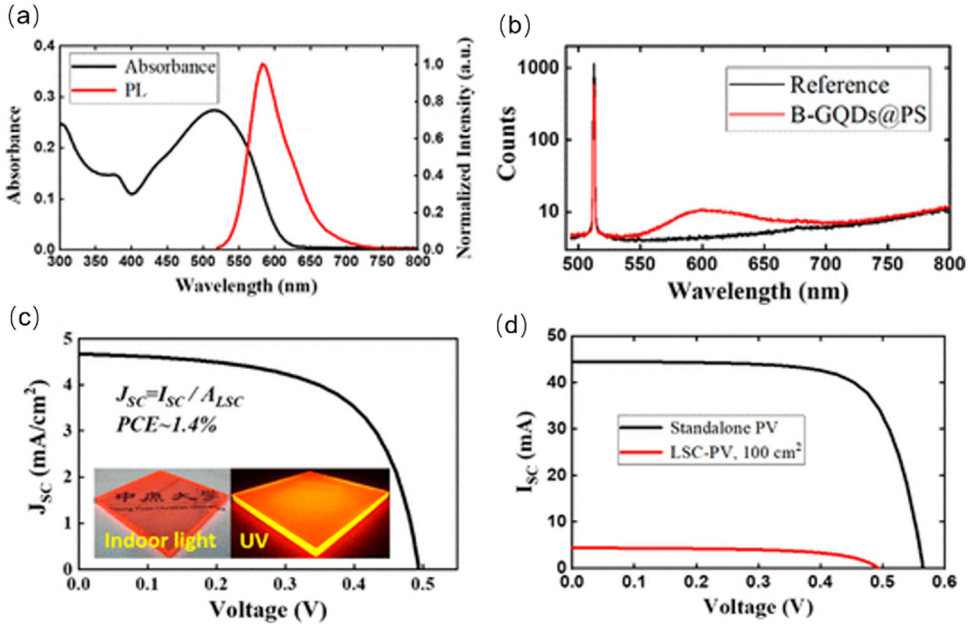

Fig. 13 (a) Absorbance and PL spectra of C-dots embedded in the PS solid matrix. (b) Experimental raw data of an absolute QY measurement. (c) The *J*–*V* curves for LSCs (100 cm^2). (d) The *J*–*V* curves for standalone PVs and LSCs–PVs. Reproduced with permission from ref. 175. Copyright 2022, American Chemical Society.

4.3 Photocatalysis

Nowadays, environmental and energy-related problems are increasingly pressing our society. The extensive use of fossil fuels, which is still the primary energy source in use and environmental pollutants are the main issues to be faced. Photocatalysis has been considered one of the most promising green chemical pathways for energy conversion and environmental pollution control, such as water remediation.[59] The creation of ROS (reactive oxygen species) is the basis for the photocatalytic process, which is normally generated on a semiconductor surface through the photoexcitation of an electron by an electromagnetic radiation with suitable energy (Fig. 10c). Thus, photocatalysis is a light-mediated advanced oxidation process where a semiconductor is implied. Conventional photocatalysts, such as TiO_2, ZnO, WO_3, $BiPO_4$, Bi_2O_3, BiOX (where X = Cl, I, and Br) and $BiVO_4$, are showing poor catalytic performances due to their wide bandgap, weak solar light absorption and fast charge recombination.[49,54,56,57,60,61,63,73] For this reason, one of the proposed solutions to overcome the limited light absorption dictated by the wide bandgap of the most effective photocatalysts is the sensitization with optically active materials, able to absorb radiation in the visible range, matching as much as possible the solar spectrum. In parallel to strong visible absorption, the sensitizers must be able to transfer the photogenerated charges to the semiconducting network with minimal charge losses. C-Dots are considered outstanding electron acceptors and donors; hence they can efficiently decrease the electrons and holes recombination process. In the design of an innovative and efficient photocatalyst, C-dots can be employed such as electron mediators, photosensitizers, photocenters, spectral converters, catalytic centers and photocatalyst themselves.[19,22,59,66] In particular, red/NIR C-dots offer new possibilities for photocatalytic applications, including the exploitation of up-conversion processes that allows in extending the absorption wavelength from visible up to NIR/IR regions and, consequently, to fully work under solar light irradiation, the most abundant renewable energy source. Since red/NIR C-dots have been regarded as promising co-catalyst, to boost the bare photocatalyst properties, and photocatalyst themselves, in this section, we consider applications in photocatalysis for both pure C-dot photocatalyst and C-dot-based composite systems. It is worth mentioning the alkali assisted electrochemical method used by Li and collaborators,[18] to obtain C-dots with up-conversion photoluminescence. They used C-dots as efficient NIR light-driven photocatalysts to selectively oxidize benzyl alcohol to benzaldehyde in the presence of H_2O_2 as the oxidant. In this regard, an interesting system reported by Wang and coworkers[176] is the full spectrum light driven C-dot modified monolayer Bi_2WO_6 nanosheet (C-dots/m-BWO) hybrid material, for the photodegradation of methyl orange (MO) and bisphenol A (BPA). According to the literature, monolayer Bi_2WO_6 nanosheets generally have an absorption below 450 nm, due to its energy gap. Instead, the heterojunction C-dots/m-BWO displayed a wider absorption up to 800 nm, suggesting that C-dots enhanced the sunlight absorption thanks to their ability to absorb the NIR light and the up-conversion effect. Furthermore, steady-state PL analysis revealed that in the C-dot/m-BWO hybrid materials the separation rate of photoinduced electron and hole pairs is higher, indicating that C-dots can act as trap for electrons emitted from m-BWO particles. As a result, the introduction of C-dots not only is helpful to improve the use of the whole solar light spectrum, but also improves the effective charge separation on

Bi_2WO_6, thus increasing the overall photocatalytic activity. C-Dots with enhanced photocatalytic activity can also be obtained through doping strategies, using different elements as electron donors, including N. For instance, Ortega-Liebana and coworkers obtained N-doped C-dots by simply using a hydrothermal method.[177] In this work, N-C-dots showed interesting and tunable emission properties, such as the capability to work both as down-converters and, in particular, as up-converting QDs. The up-conversion effect has been ascribed to their ability to absorb longer wavelengths by emitting shorter wavelengths in a multi-photon absorption event. In fact, it is usually accepted that doping atoms are providing intermediate energy levels, which favor the direct or sequential absorption of two lower energy photons (higher wavelengths) to give emission at higher energy (shorter wavelengths).[178] Therefore, N-doped C-dots exhibit an enhanced photo-response in the NIR region, and they are promising to be used in a wider range spectrum. Remarkably, N-C-dots from the same study were able to improve the optical properties of a commercial anatase photocatalyst and consequently to increase the photocatalytic activity for the photodegradation of a well-known pesticide (2,4-dichlorophenol, DCP) under visible light. As stated, the C-dot emission at a higher wavelength region is influenced by the incorporation or doping of heteroatoms and this is a common effect confirmed in many published reports on this topic.[78,127,179] Furthermore, one of the greatest advantages on the use of C-dots is the possibility to obtain them using environmentally friendly precursor materials, especially today that the green approach is gaining more attention. In this regard, low-cost C-dots can be obtained by directly using a natural source without external chemical reagents such as lemon juice, mango leaves or, in the case of red-emitting magnesium–nitrogen embedded C-dots (r-Mg–N-C-dots), Bougainvillea leaves.[38,77] r-Mg–N-C-dots were tested for the photocatalytic degradation of methylene blue (MB) dye under sunlight irradiation. They can reach high photocatalytic activity and MB is 99.1% photodegraded within about 120 minutes thanks to the presence of several surface functional states, which give the ability of r-Mg–N-C-dots to absorb different excitation wavelengths (~270, ~325, ~420 and ~674 nm). Therefore, the incorporation or doping of heteroatoms such as Mg and N in the graphitic carbon framework of C-dots give rise to red fluorescence, which is independent from the excitation wavelengths. In a more recent study, N-C-dots have been used to obtain a broad-spectrum-driven heterojunction in combination with $Bi_2O_2CO_3$ (BOC).[180] N-C-Dots can be excited by different long-wavelengths (650–900 nm) resulting in up-converted PL at shorter wavelengths (450–550 nm), enhancing the light absorption in the visible and NIR regions of the overall BOC/NCQDs system, thus realizing an efficient photodegradation of ciprofloxacin (CIP). N-C-dots may have two different roles for the CIP degradation according to the light-source used (Fig. 14). Z-Scheme electron transfer pathway may occur under UV light irradiation, while the type-II electron transfer pathway under visible and NIR light irradiation. Consequently, N-C-dots can act as electron supplies in the case of Z-scheme working under UV light and both as photosensitizers and hole sources if irradiated with visible and NIR light (type-II scheme).

Another remarkable example on the use of N doped C-dots to enhance the full-spectrum photocatalytic activity by designing an appropriate heterojunction is the Ag@N-CQD core–shell modified $BiVO_4$ system proposed by Zhang and coworkers.[74]

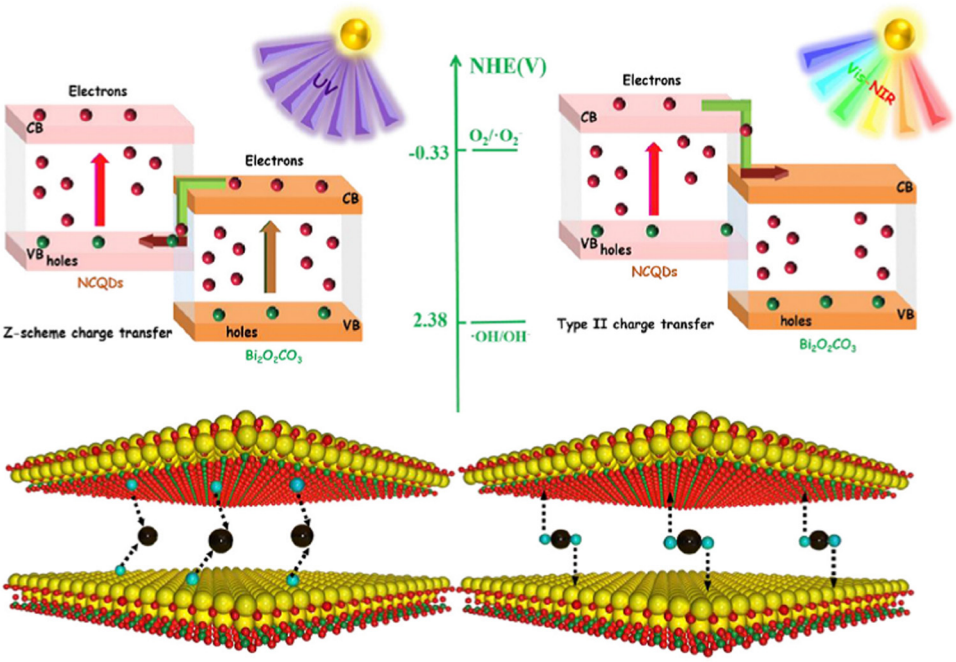

Fig. 14 Schematic diagram of different N-C-dots/BOC heterojunctions and two different roles of N-C-dots under UV, visible and NIR light irradiation. Reproduced with permission from ref. 180. Copyright 2021, Elsevier Ltd.

The optical properties of the whole system are improved by the Ag@N-C-dot core–shell structures, which exhibit an extended light absorption region from 320 nm up to 800 nm thanks to the synergistic effect between Ag and N-C-dots. The up-conversion effect makes the N-C-dots able to absorb a long wavelength light (700–900 nm) with up-converted emissions located in the range of 400–600 nm, which can be further employed by Ag nanoparticles with an enhancement on surface plasmon resonance (SPR) effect. Consequently, the Ag@N-C-dot core–shell structures act as an energy transfer component in the $BiVO_4$/Ag@N-C-dot heterojunction with an increased absorption up to the NIR region. Lastly, the good results reached in the tetracycline hydrochloride (TC) removal suggest that the improved photocatalytic activity of $BiVO_4$/Ag@N-C-dots is clearly due to the presence of the C-dot up-conversion effect in combination with the Ag SPR effect, which are providing long-wavelength Vis-NIR light absorption, high efficiency of charge separation and strong oxidation ability.

5. Conclusions and perspectives

In this review, we focused on red/NIR C-dots. We summarized the most recent methods for their synthesis, including hydrothermal, solvothermal, microwave-assisted and pyrolysis approaches using various types of precursors, such as CA–urea and aromatic compounds. We stressed the importance to control the C-dot carbonization degree by adjusting synthetic conditions. To obtain the accurate characterization of the optoelectronic properties of C-dots, TA and transient PL spectra could be used as efficient tools to study the exciton dynamics in C-dots, which plays a major role in determining their photocatalytic properties. These tools not only help to understand the PL mechanisms, but also can give guidance for the optimization of the functional properties of the C-dots, for optical and optoelectronic applications. The toxicity of red-NIR C-dots is an important issue to be assessed, since prospective applications of these nanostructures include nanothermometry and bioimaging, in which cytotoxicity is critical. In addition, the peculiar optical properties of red/NIR C-dots make them suitable for other different applications, including photocatalysis and LSCs. Specific applications call for specific optical features. For example, nanothermometry needs the C-dots have two emission peaks with different PL responses as a function of the temperature. LSCs require the C-dots have a large Stokes shift (a small spectral overlap between the absorption and emission) to minimize reabsorption, together with broad absorption and high QY. Photocatalytic applications need the C-dots have broad absorption and band energy levels suitable for the efficient charge separation and transfer.

Although great achievements have been obtained on the synthesis, optoelectronic properties and applications of red/NIR C-dots, several major issues still exist that need to be urgently solved. (i) Only few reports describe red/NIR C-dots with stable emission and broad absorption. Further research should focus on the selection of aromatic compounds for highly carbonized C-dots with emission at long wavelengths (700–1400 nm). A reliable and reproducible approach is still absent for large-scale synthesis. In addition, it is also a challenge to produce C-dots in large-scale, maintaining controlled optical properties. Furthermore, standard protocols for the post-purification procedure of C-dots are not clearly identified. (ii) The QY continues to be a great challenge, still being relatively low especially for C-dots with NIR emission. The exciton dynamics in red/NIR C-dots represents an important aspect, which deserves to be further analyzed to elucidate the processes of charge separation and transfer. However, as stated in this review, it has been demonstrated that ultrafast optical spectroscopies may be a powerful tool. (iii) The functional properties of the devices based on red/near infrared C-dots are still not high; hence, they need to be further improved. In addition, the long-term operation stability should be investigated. (iv) For the potential commercialization of red/NIR C-dots for LSCs and photocatalysis, the PCE or solar-to-fuel conversion efficiency is still low and the detailed study for the cost of devices is still lacking. Further challenges lie in the improvement of the functional properties of the C-dots, such as the QY and absorption/emission range and simple synthetic approach using low-cost precursors. Clarifying these issues requires a deep investigation of the structure and optoelectrical variations that occur during the device operation.

In conclusion, the future research direction for red/NIR C-dots may focus on the (i) large-scale synthesis of C-dots with broad absorption and a very high QY (up to 100%) through doping, surface post-treatment and high crystal structure engineering; (ii) deeper understanding of the exciton/charge dynamics for the C-dots with different sizes, shapes, compositions and surface functional groups; (iii) improving the device performance by appropriate tailoring of the structure and optical/optoelectronic properties of the C-dots and optimizing the interaction/energy level alignment between C-dots and the other materials in the devices.

Conflicts of interest

There are no conflicts to declare.

Acknowledgements

This work was supported by the Shandong Natural Science Funds for Distinguished Young Scholar (ZR2020JQ20) and the Key Research and Development Program of Shandong Province (Grant No. 2021CXGC011003). A. V. acknowledges the Kempe Foundation and the Knut & Alice Wallenberg Foundation for financial support.

References

1 A. L. Efros, *Nature*, 2019, **575**, 604.
2 H. Lu, Z. Huang, M. S. Martinez, J. C. Johnson, J. M. Luther and M. C. Beard, *Energy Environ. Sci.*, 2020, **13**, 1347.

3 G. S. Selopal, H. Zhao, X. Tong, D. Benetti, F. Navarro-Pardo, Y. Zhou, D. Barba, F. Vidal, Z. M. Wang and F. Rosei, *Adv. Funct. Mater.*, 2017, **27**, 1701468.
4 Y. Shu, X. Lin, H. Qin, Z. Hu, Y. Jin and X. Peng, *Angew. Chem., Int. Ed.*, 2020, **59**, 22312.
5 K. Wu, H. Li and V. I. Klimov, *Nat. Photonics*, 2018, **12**, 105.
6 W. Zhou, Y. Shang, F. P. G. de Arquer, K. Xu, R. Wang, S. Luo, X. Xiao, X. Zhou, R. Huang, E. H. Sargent and Z. Ning, *Nat. Electron.*, 2020, **3**, 251.
7 E. M. K. Akbar and A. Vomiero, *Adv. Opt. Mater.*, 2021, **9**, 2100532.
8 C. Campalani, S. Zorzi, A. Vomiero, S. You, L. Matthews, M. Capron, C. Mondelli, M. Selva and A. Perosa, *Nanomater*, 2021, **11**, 524.
9 S. Cailotto, F. Enrichi, A. Vomiero, M. Selva, E. Cattaruzza, D. Cristofori, E. Amadio and A. Perosa, *ACS Appl. Mater. Interfaces*, 2018, **10**, 40560.
10 G. Liu, H. Zhao, F. Diao, Z. Ling and Y. Wang, *J. Mater. Chem. C*, 2018, **6**, 10059.
11 H. Zhao, D. Benetti, X. Tong, H. Zhang, Y. Zhou, G. Liu, D. Ma, S. Sun, Z. M. Wang, Y. Wang and F. Rosei, *Nano Energy*, 2018, **50**, 756.
12 X. Y. Xu, R. Ray, Y. L. Gu, H. J. Ploehn, L. Gearheart, K. Raker and W. A. Scrivens, *J. Am. Chem. Soc.*, 2004, **126**, 12736.
13 S. N. Baker and G. A. Baker, *Angew. Chem., Int. Ed.*, 2010, **49**, 6726.
14 H. T. Li, Z. H. Kang, Y. Liu and S.-T. Lee, *J. Mater. Chem.*, 2012, **22**, 24230.
15 Z. P. Zhang, J. Zhang, N. Chen and L. T. Qu, *Energy Environ. Sci.*, 2012, **5**, 8869.
16 J. Bartelmess, S. J. Quinn and S. Giordani, *Chem. Soc. Rev.*, 2015, **44**, 4672.
17 S. Sarkar, D. Banerjee, U. K. Ghorai, N. S. Das and K. K. Chattopadhyay, *J. Lumin.*, 2016, **178**, 314.
18 H. Li, R. Liu, S. Lian, Y. Liu, H. Huang and Z. Kang, *Nanoscale*, 2013, **5**, 3289.
19 Y. Wang and A. Hu, *J. Mater. Chem. C*, 2014, **2**, 6921.
20 S. Y. Lim, W. Shen and Z. Q. Gao, *Chem. Soc. Rev.*, 2015, **44**, 362.
21 M. Li, R. Zhao, Y. Su, Z. Yang and Y. Zhang, *Nanoscale*, 2016, **8**, 8559.
22 R. Wang, K. Q. Lu, Z. R. Tang and Y. J. Xu, *J. Mater. Chem. A*, 2017, **5**, 3717.
23 Z. Wang, F. Yuan, X. Li, Y. Li, H. Zhong, L. Fan and S. Yang, *Adv. Mater.*, 2017, **29**, 1702910.
24 K.-H. Ye, Z. Wang, J. Gu, S. Xiao, Y. Yuan, Y. Zhu, Y. Zhang, W. Mai and S. Yang, *Energy Environ. Sci.*, 2017, **10**, 772.
25 F. Yuan, Z. Wang, X. Li, Y. Li, Z. Tan, L. Fan and S. Yang, *Adv. Mater.*, 2017, **29**, 1604436.
26 W. Li, Y. Liu, M. Wu, X. Feng, S. A. T. Redfern, Y. Shang, X. Yong, T. Feng, K. Wu, Z. Liu, B. Li, Z. Chen, J. S. Tse, S. Lu and B. Yang, *Adv. Mater.*, 2018, **30**, 1800676.
27 D. Benetti, E. Jokar, C.-H. Yu, A. Fathi, H. Zhao, A. Vomiero, E. W. G. Diau and F. Rosei, *Nano Energy*, 2019, **62**, 781.
28 H. Zhao, *J. Lumin.*, 2019, **211**, 150.
29 H. Zhao, G. Liu and G. Han, *Nanoscale Adv.*, 2019, **1**, 4888.
30 G. Liu, X. Wang, G. Han, J. Yu and H. Zhao, *Mater. Adv.*, 2020, **1**, 119.
31 Y. Han, Y. Liu, H. Zhao, A. Vomiero and R. Li, *J. Mater. Chem. B*, 2021, **9**, 4111.
32 Y. Han, X. Zhao, A. Vomiero, X. Gong and H. Zhao, *J. Mater. Chem. C*, 2021, **9**, 12255.
33 J. Li, H. Zhao, X. Zhao and X. Gong, *Nanoscale*, 2021, **13**, 9561.
34 S. Ren, B. Liu, G. Han, H. Zhao and Y. Zhang, *Nanoscale*, 2021, **13**, 12149.
35 X. Wang, M. Wang, G. Liu, Y. Zhang, G. Han, A. Vomiero and H. Zhao, *Nano Energy*, 2021, **86**, 106122.
36 H. Zhao, G. Liu, S. You, F. V. A. Camargo, M. Zavelani-Rossi, X. Wang, C. Sun, B. Liu, Y. Zhang, G. Han, A. Vomiero and X. Gong, *Energy Environ. Sci.*, 2021, **14**, 396.
37 X. Bao, Y. Yuan, J. Chen, B. Zhang, D. Li, D. Zhou, P. Jing, G. Xu, Y. Wang, K. Hola, D. Shen, C. Wu, L. Song, C. Liu, R. Zboril and S. Qu, *Light: Sci. Appl.*, 2018, **7**, 91.
38 A. Bhati, S. R. Anand, Gunture, A. K. Garg, P. Khare and S. K. Sonkar, *ACS Sustainable Chem. Eng.*, 2018, **6**, 9246.
39 B. Yuan, S. Guan, X. Sun, X. Li, H. Zeng, Z. Xie, P. Chen and S. Zhou, *ACS Appl. Mater. Interfaces*, 2018, **10**, 16005.
40 H. Jia, Z. Wang, T. Yuan, F. Yuan, X. Li, Y. Li, Z. Tan, L. Fan and S. Yang, *Adv. Sci.*, 2019, **6**, 1900397.
41 T. Meng, T. Yuan, X. Li, Y. Li, L. Fan and S. Yang, *Chem. Commun.*, 2019, **55**, 6531.
42 P. He, Y. Shi, T. Meng, T. Yuan, Y. Li, X. Li, Y. Zhang, L. Fan and S. Yang, *Nanoscale*, 2020, **12**, 4826.
43 F. Yuan, Y.-K. Wang, G. Sharma, Y. Dong, X. Zheng, P. Li, A. Johnston, G. Bappi, J. Z. Fan, H. Kung, B. Chen, M. I. Saidaminov, K. Singh, O. Voznyy, O. M. Bakr, Z. H. Lu and E. H. Sargent, *Nat. Photonics*, 2020, **14**, 171.
44 T. Meng, Z. Wang, T. Yuan, X. Li, Y. Li, Y. Zhang and L. Fan, *Angew. Chem., Int. Ed.*, 2021, **60**, 16343.
45 Y. Shi, Z. Wang, T. Meng, T. Yuan, R. Ni, Y. Li, X. Li, Y. Zhang, Z. Tan, S. Lei and L. Fan, *J. Am. Chem. Soc.*, 2021, **143**, 18941.
46 Y. Li, P. Miao, W. Zhou, X. Gong and X. Zhao, *J. Mater. Chem. A*, 2017, **5**, 21452.
47 G. Zhang, Q. Ji, Z. Wu, G. Wang, H. Liu, J. Qu and J. Li, *Adv. Funct. Mater.*, 2018, **28**, 1706462.
48 D. Luo, Q. Chen, Y. Qiu, B. Liu and M. Zhang, *Mater.*, 2019, **12**, 1713.
49 S. Qiu, Y. Shen, G. Wei, S. Yao, W. Xi, M. Shu, R. Si, M. Zhang, J. Zhu and C. An, *Appl. Catal., B*, 2019, **259**, 118036.
50 J. Wang, J. Wang, Y. Xu, J. Jin, W. Xiao, D. Tan, J. Li, T. Mei, L. Xue and X. Wang, *ACS Appl. Energy Mater.*, 2020, **3**, 12230.
51 L. Zdrazil, S. Kalytchuk, K. Hola, M. Petr, O. Zmeskal, S. Kment, A. L. Rogach and R. Zboril, *Nanoscale*, 2020, **12**, 6664.
52 Indriyati, I. Primadona, F. A. Permatasari, M. A. Irham, M. Nasir and F. Iskandar, *Nanoscale*, 2021, **13**, 7523.
53 C. Yang, W. Sheng, M. Moemeni, M. Bates, C. K. Herrera, B. Borhan and R. R. Lunt, *Adv. Energy Mater.*, 2021, **11**, 2003581.

54 Q. Wang, J. Hui, Y. Huang, Y. Ding, Y. Cai, S. Yin, Z. Li and B. Su, *Mater. Sci. Semicond. Process.*, 2014, **17**, 87.
55 Y. Liu, W. Yao, D. Liu, R. Zong, M. Zhang, X. Ma and Y. Zhu, *Appl. Catal., B*, 2015, **163**, 547.
56 P. Chen, F. Wang, Z. F. Chen, Q. Zhang, Y. Su, L. Shen, K. Yao, Y. Liu, Z. Cai, W. Lv and G. Liu, *Appl. Catal., B*, 2017, **204**, 250.
57 W. Shi, F. Guo, C. Zhu, H. Wang, H. Li, H. Huang, Y. Liu and Z. Kang, *J. Mater. Chem. A*, 2017, **5**, 19800.
58 H. L. Tan, R. Amal and Y. H. Ng, *J. Mater. Chem. A*, 2017, **5**, 16498.
59 M. Han, S. Zhu, S. Lu, Y. Song, T. Feng, S. Tao, J. Liu and B. Yang, *Nano Today*, 2018, **19**, 201.
60 T. Hu, Y. Yang, K. Dai, J. Zhang and C. Liang, *Appl. Surf. Sci.*, 2018, **456**, 473.
61 L. Jiang, X. Yuan, G. Zeng, J. Liang, X. Chen, H. Yu, H. Wang, Z. Wu, J. Zhang and T. Xiong, *Appl. Catal., B*, 2018, **227**, 376.
62 Y. Wang, X. Liu, J. Liu, B. Han, X. Hu, F. Yang, Z. Xu, Y. Li, S. Jia, Z. Li and Y. Zhao, *Angew. Chem., Int. Ed.*, 2018, **57**, 5765.
63 Q. Zhang, P. Chen, M. Zhuo, F. Wang, Y. Su, T. Chen, K. Yao, Z. Cai, W. Lv and G. Liu, *Appl. Catal., B*, 2018, **221**, 129.
64 M. Zhu, X. Deng, X. Lin, L. Zhang, W. Zhang, Y. Lv and J. Pan, *J. Mater. Sci.: Mater. Electron.*, 2018, **29**, 11449.
65 I. Sargin, G. Yanalak, G. Arslan and I. H. Patir, *Int. J. Hydrogen Energy*, 2019, **44**, 21781.
66 S. Sharma, V. Dutta, P. Singh, P. Raizada, A. Rahmani-Sani, A. Hosseini-Bandegharaei and V. K. Thakur, *J. Cleaner Prod.*, 2019, **228**, 755.
67 T. Xu, D. Wang, L. Dong, H. Shen, W. Lu and W. Chen, *Appl. Catal., B*, 2019, **244**, 96.
68 D. S. Achilleos, H. Kasap and E. Reisner, *Green Chem.*, 2020, **22**, 2831.
69 X. Meng, C. Zhang, C. Dong, W. Sun, D. Ji and Y. Ding, *Chem. Eng. J.*, 2020, **389**, 124432.
70 Q. Wang, J. Cai, G. V. Biesold-McGee, J. Huang, Y. H. Ng, H. Sun, J. Wang, Y. Lai and Z. Lin, *Nano Energy*, 2020, **78**, 105313.
71 Y. Yang, M. Qiu, Q. Qi, F. Chen, J. Chen, Y. Liu and L. Yang, *ACS Appl. Nano Mater*, 2020, **3**, 10296.
72 Z. Zhang, G. Yi, P. Li, X. Zhang, H. Fan, Y. Zhang, X. Wang and C. Zhang, *Nanoscale*, 2020, **12**, 13899.
73 J. C. Murillo-Sierra, A. Hernández-Ramírez, L. Hinojosa-Reyes and J. L. Guzmán-Mar, *Chem. Eng. J. Adv.*, 2021, **5**, 100070.
74 J. Zhang, M. Si, L. Jiang, X. Yuan, H. Yu, Z. Wu, Y. Li and J. Guo, *Chem. Eng. J.*, 2021, **410**, 28336.
75 L. J. Mohammed and K. M. Omer, *Nanoscale Res. Lett.*, 2020, **15**, 182.
76 H. Ding, J. S. Wei, N. Zhong, Q. Y. Gao and H.-M. Xiong, *Langmuir*, 2017, **33**, 12635.
77 M. K. Kumawat, M. Thakur, R. B. Gurung and R. Srivastava, *ACS Sustainable Chem. Eng.*, 2017, **5**, 1382.
78 Y. Liu, W. Duan, W. Song, J. Liu, C. Ren, J. Wu, D. Liu and H. Chen, *ACS Appl. Mater. Interfaces*, 2017, **9**, 12663.
79 W. Shi, F. Guo, M. Han, S. Yuan, W. Guan, H. Li, H. Huang, Y. Liu and Z. Kang, *J. Mater. Chem. B*, 2017, **5**, 3293.
80 L. Wei, Y. Ma, X. Shi, Y. Wang, X. Su, C. Yu, S. Xiang, L. Xiao and B. Chen, *J. Mater. Chem. B*, 2017, **5**, 3383.
81 B. B. Karakocak, J. Liang, S. Kavadiya, M. Y. Berezin, P. Biswas and N. Ravi, *ACS Appl. Nano Mater.*, 2018, **1**, 3682.
82 M. Xue, J. Zhao, Z. Zhan, S. Zhao, C. Lan, F. Ye and H. Liang, *Nanoscale*, 2018, **10**, 18124.
83 H. Ding, X. Zhou, B. Qin, Z. Zhou and Y. Zhao, *J. Lumin.*, 2019, **211**, 298.
84 X. Shi, H. Meng, Y. Sun, L. Qu, Y. Lin, Z. Li and D. Du, *Small*, 2019, **15**, 1901507.
85 Y. Wen, Q. Jia, F. Nan, X. Zheng, W. Liu, J. Wu, H. Ren, J. Ge and P. Wang, *Chem. – Asian J.*, 2019, **14**, 2162.
86 H. Ding, X. X. Zhou, J. S. Wei, X. B. Li, B. T. Qin, X. B. Chen and H. M. Xiong, *Carbon*, 2020, **167**, 322.
87 K. Hola, M. V. Pavliuk, B. Nemeth, P. Huang, L. Zdrazil, H. Land, G. Berggren and H. Tian, *ACS Catal.*, 2020, **10**, 9943.
88 B. B. Karakocak, A. Laradji, T. Primeau, M. Y. Berezin, S. Li and N. Ravi, *ACS Appl. Mater. Interfaces*, 2021, **13**, 277.
89 S. Li, W. Su, H. Wu, T. Yuan, C. Yuan, J. Liu, G. Deng, X. Gao, Z. Chen, Y. Bao, F. Yuan, S. Zhou, H. Tan, Y. Li, X. Li, L. Fan, J. Zhu, A. T. Chen, F. Liu, Y. Zhou, M. Li, X. Zhai and J. Zhou, *Nat. Biomed. Eng.*, 2020, **4**, 704.
90 Y. Liu, H. Gou, X. Huang, G. Zhang, K. Xi and X. Jia, *Nanoscale*, 2020, **12**, 1589.
91 Z. M. Markovic, M. Labudova, M. Danko, D. Matijasevic, M. Micusik, V. Nadazdy, M. Kovacova, A. Kleinova, Z. Spitalsky, V. Pavlovic, D. D. Milivojevic, M. Medic and B. M. T. Markovic, *ACS Sustainable Chem. Eng.*, 2020, **8**, 16327.
92 Y.-P. Sun, B. Zhou, Y. Lin, W. Wang, K. A. S. Fernando, P. Pathak, M. J. Meziani, B. A. Harruff, X. Wang, H. Wang, P. G. Luo, H. Yang, M. E. Kose, B. Chen, L. M. Veca and S.-Y. Xie, *J. Am. Chem. Soc.*, 2006, **128**, 7756–7757.
93 Q. L. Zhao, Z. L. Zhang, B. H. Huang, J. Peng, M. Zhang and D. W. Pang, *Chem. Commun.*, 2008, 5116–5118.
94 F. Yuan, P. He, Z. Xi, X. Li, Y. Li, H. Zhong, L. Fan and S. Yang, *Nano Res.*, 2019, **12**, 1669.
95 L. Lin and S. Zhang, *Chem. Commun.*, 2012, **48**, 10177–10179.
96 H. Ding, Y. Ji, J.-S. Wei, Q.-Y. Gao, Z.-Y. Zhou and H.-M. Xiong, *J. Mater. Chem. B*, 2017, **5**, 5272.
97 H. Ding, J. S. Wei, P. Zhang, Z. Y. Zhou, Q. Y. Gao and H. M. Xiong, *Small*, 2018, **14**, 1800612.
98 S. Lu, L. Sui, M. Wu, S. Zhu, X. Yong and B. Yang, *Adv. Sci.*, 2019, **6**, 1801192.
99 C. Xia, S. Zhu, T. Feng, M. Yang and B. Yang, *Adv. Sci.*, 2019, **6**, 1901316.
100 T. Feng, S. Tao, D. Yue, Q. Zeng, W. Chen and B. Yang, *Small*, 2020, **16**, 2001295.
101 D. Zhou, P. Jing, Y. Wang, Y. Zhai, D. Li, Y. Xiong, A. V. Baranov, S. Qu and A. L. Rogach, *Nanoscale Horiz.*, 2019, **4**, 388.
102 M. Lan, S. Zhao, Z. Zhang, L. Yan, L. Guo, G. Niu, J. Zhang, J. Zhao, H. Zhang, P. Wang, G. Zhu, C. S. Lee and W. Zhang, *Nano Res.*, 2017, **10**, 3113.

103 D. Li, P. Jing, L. Sun, Y. An, X. Shan, X. Lu, D. Zhou, D. Han, D. Shen, Y. Zhai, S. Qu, R. Zboril and A. L. Rogach, *Adv. Mater.*, 2018, **30**, 1705913.
104 F. A. Permatasari, H. Fukazawa, T. Ogi, F. Iskandar and K. Okuyama, *ACS Appl. Nano Mater.*, 2018, **1**, 2368.
105 D. Li, C. Liang, E. V. Ushakova, M. Sun, X. Huang, X. Zhang, P. Jing, S. J. Yoo, J.-G. Kim, E. Liu, W. Zhang, L. Jing, G. Xing, W. Zheng, Z. Tang, S. Qu and A. L. Rogach, *Small*, 2019, **15**, 1905050.
106 H. Liu, X. Lv, J. Qian, H. Li, Y. Qian, X. Wang, X. Meng, W. Lin and H. Wang, *ACS Nano*, 2020, **14**, 13304.
107 C. L. Shen, Q. Lou, J. H. Zang, K. K. Liu, S. N. Qu, L. Dong and C. X. Shan, *Adv. Sci.*, 2020, **7**, 1903525.
108 X. Chu, P. Zhang, Y. Wang, B. Sun, Y. Liu, Q. Zhang, W. Feng, Z. Li, K. Li, N. Zhou and J. Shen, *Carbon*, 2021, **176**, 126.
109 D. Li, E. V. Ushakova, A. L. Rogach and S. Qu, *Small*, 2021, **17**, 2102325.
110 F. Nan, X. Xue, J. Ge and P. Wang, *Chin. J. Lumin.*, 2021, **42**, 1155.
111 X. Lu, S. Xie, H. Yang, Y. Tong and H. Ji, *Chem. Soc. Rev.*, 2014, **43**, 7581.
112 C. Li, Y. Wang, H. Jiang and X. Wang, *J. Electrochem. Soc.*, 2020, **167**, 037540.
113 F. Yuan, S. Li, Z. Fan, X. Meng, L. Fan and S. Yang, *Nano Today*, 2016, **11**, 565.
114 K. J. Mintz, Y. Zhou and R. M. Leblanc, *Nanoscale*, 2019, **11**, 4634.
115 B. K. Walther, C. Z. Dinu, D. M. Guldi, V. G. Sergeyev, S. E. Creager, J. P. Cooke and A. Guiseppi-Elie, *Mater. Today*, 2020, **39**, 23.
116 D. Xu, Q. Lin and H.-T. Chang, *Small Methods*, 2020, **4**, 1900387.
117 L. Ansari, S. Hallaj, T. Hallaj and M. Amjadi, *Colloids Surf., B*, 2021, **203**, 111743.
118 J. Ge, Q. Jia, W. Liu, L. Guo, Q. Liu, M. Lan, H. Zhang, X. Meng and P. Wang, *Adv. Mater.*, 2015, **27**, 4169.
119 I. Concina, Z. H. Ibupoto and A. Vomiero, *Adv. Energy Mater.*, 2017, **7**, 1770138.
120 X. Miao, D. Qu, D. Yang, B. Nie, Y. Zhao, H. Fan and Z. Sun, *Adv. Mater.*, 2018, **30**, 1870002.
121 B. Yang, R. Jelinek and Z. H. Kang, *Mater. Chem. Front.*, 2020, **4**, 1287–1288.
122 Y. Liu, H. Huang, W. Cao, B. Mao, Y. Liu and Z. H. Kang, *Mater. Chem. Front.*, 2020, **4**, 1586–1613.
123 Q. Zhao, W. Song, B. Zhao and B. Yang, *Mater. Chem. Front.*, 2020, **4**, 472–488.
124 D. Qu and Z. Sun, *Mater. Chem. Front.*, 2020, **4**, 400–420.
125 H. Zhang, J. Liu, B. Wang, K. Liu, G. Chen, X. Yu, J. Li and J. H. Yu, *Mater. Chem. Front.*, 2020, **4**, 1404–1410.
126 Z. Zhang, W. Sun and P. Wu, *ACS Sustainable Chem. Eng.*, 2015, **3**, 1412.
127 F. Arcudi, L. Dordevic and M. Prato, *Angew. Chem., Int. Ed.*, 2016, **55**, 2107.
128 T. Bao, L. Song and S. Zhang, *Chem. Eng. J.*, 2018, **351**, 189.
129 S. Paul, S. Ghosh, B. Dalal, P. Chal, B. Satpati and S. K. De, *Chem. Mater.*, 2018, **30**, 5020.
130 B. Zhi, X. Yao, Y. Cui, G. Orr and C. L. Haynes, *Nanoscale*, 2019, **11**, 20411.
131 G. Magdy, A. F. Abdel Hakiem, F. Belal and A. M. Abdel-Megied, *Food Chem.*, 2020, **343**, 128539.
132 S. Y. Song, L. Z. Sui, K. K. Liu, Q. Cao, W. B. Zhao, Y. C. Liang, C. F. Lv, J. H. Zang, Y. Shang, Q. Lou, X. G. Yang, L. Dong, K. J. Yuan and C. X. Shan, *Nano Res.*, 2021, **14**, 2231.
133 Z. Zhang and H. Wu, *RSC Adv.*, 2014, **4**, 37395.
134 K. Hola, M. Sudolska, S. Kalytchuk, D. Nachtigallova, A. L. Rogach, M. Otyepka and R. Zboril, *ACS Nano*, 2017, **11**, 12402.
135 F. Yuan, T. Yuan, L. Sui, Z. Wang, Z. Xi, Y. Li, X. Li, L. Fan, Z. Tan, A. Chen, M. Jin and S. Yang, *Nat. Commun.*, 2018, **9**, 2249.
136 K. K. Liu, S. Y. Song, L. Z. Sui, S. X. Wu, P. T. Jing, R. Q. Wang, Q. Y. Li, G. R. Wu, Z. Z. Zhang, K. J. Yuan and C. X. Shan, *Adv. Sci.*, 2019, **4**, 1900766.
137 Z. Zhang, X. Chen, G. Fang, J. Wu and A. L. Gao, *J. Mater. Chem. C*, 2022, **10**, 3153.
138 X. Q. Niu, T. Song and H. M. Xiong, *Chin. Chem. Lett.*, 2021, **32**, 1953.
139 Z. He, S. Liu, C. Zhang, L. Fan, J. Zhang, Q. Chen, Y. Sun, L. He, Z. Wang and K. Zhang, *Nano Sel.*, 2021, **2**, 1589.
140 R. Q. Ye, Z. W. Peng, A. Metzger, J. Lin, J. A. Mann, K. W. Huang, C. S. Xiang, X. J. Fan, E. L. G. Samuel, L. B. Alemany, A. A. Martí and J. M. Tour, *ACS Appl. Mater. Interfaces*, 2015, **7**, 7041.
141 Q. Q. Ran, X. P. Wang, P. Ling, P. Yan, J. Xu, L. Jiang, Y. Wang, S. Su, S. Hu and J. Xiang, *Carbon*, 2022, **193**, 404.
142 M. Chen, C. Liu, Y. An, Y. Li, Y. Zheng, H. Tian, R. Shi, X. He and X. Lin, *Nanoscale Adv.*, 2022, **4**, 14.
143 J. Liu, T. Kong and H. M. Xiong, *Adv. Mater.*, 2022, **34**, 2200152.
144 X. Miao, X. Yan, D. Qu, D. Li, F. F. Tao and Z. Sun, *ACS Appl. Mater. Interfaces*, 2017, **9**, 18549.
145 Y. Zhang, H. Song, L. Wang, J. K. Yu, B. Y. Wang, Y. S. Hu, S. Q. Zang, B. Yang and S. Y. Lu, *Angew. Chem., Int. Ed.*, 2021, **60**, 25514.
146 M. Wei, K. Feng, C. Li, N. Xie, Y. Wang, X. L. Yang, B. Chen, C. H. Tung and L. Z. Wu, *Matter*, 2020, **2**, 495.
147 X. Xu, G. Hu, L. Mo, Y. Li, H. Wei, B. Lei, X. Zhang, C. F. Hu, J. Zhuang and Y. L. Liu, *Nanoscale*, 2021, **13**, 6846.
148 Y. Zheng, K. Arkin, J. Hao, S. Zhang, W. Guan, L. Wang, Y. Guo and Q. K. Shang, *Adv. Opt. Mater.*, 2021, **9**, 2100688.
149 H. S. Shim, J. M. Kim, S. Jeong, Y. Ju, S. J. Won, J. Choi, S. Nam, A. Molla, J. Kim and J. K. Song, *Nanoscale Adv.*, 2022, **4**, 1351.
150 T. Yuan, T. Meng, P. He, Y. Shi, Y. Li, X. Li, L. Fan and S. Yang, *J. Mater. Chem. C*, 2019, **7**, 6820.
151 W. Su, R. Guo, F. Yuan, Y. Li, X. Li, Y. Zhang, S. Zhou and L. Fan, *J. Phys. Chem. Lett.*, 2020, **11**, 1357.
152 J. Huang, D. Wang, S. Li, H. Fan and L. Fan, *Acta Phys. Chim. Sin.*, 2021, **37**, 1905067.
153 T. Yuan, T. Meng, Y. Shi, X. Song, W. Xie, Y. Li, X. Li, Y. Zhang and L. Fan, *J. Mater. Chem. C*, 2022, **10**, 2333.

154 C. L. Shen, Q. Lou, K. K. Liu, L. Dong and C. X. Shan, *Nano Today*, 2020, **35**, 100954.
155 S. Zhu, Y. Song, X. Zhao, J. Shao, J. Zhang and B. Yang, *Nano Res.*, 2015, **8**, 355.
156 S. Ghosh, A. Ghosh, G. Ghosh, K. Marjit and A. Patra, *J. Phys. Chem. Lett.*, 2021, **12**, 8080.
157 J. Feng, H. Dong, L. Yu and L. Dong, *J. Mater. Chem. C*, 2017, **5**, 5984.
158 S. S. Wu, H. Shi, W. Lu, S. Wei, H. Shang, H. Liu, M. Si, X. Le, G. Yin, P. Theato and T. Chen, *Angew. Chem., Int. Ed.*, 2021, **60**, 21890.151.
159 Y.-Y. Liu, N.-Y. Yu, W.-D. Fang, Q. G. Tan, R. Ji, L. Y. Yang, S. Wei, X. W. Zhang and A. J. Miao, *Nat. Commun.*, 2021, **12**, 1.
160 Q. Ji, X. Zheng, J. Ge, W. Liu, H. Ren, S. Chen, Y. Wen, H. Zhang, J. Wu and P. Wang, *J. Colloid Interface Sci.*, 2018, **526**, 302–311.
161 Y. Liu, X. Zhi, W. Hou, F. Xia, J. Zhang, L. Li, Y. Hong, H. Yan, C. Peng, J. M. de la Fuentea, J. Song and D. Cui, *Nanoscale*, 2018, **10**, 19052.
162 T. Malina, K. Polakova, J. Skopalik, V. Milotova, K. Hola, M. Havrdova, K. B. Tomankova, V. Cmiel, L. Sefc and R. Zboril, *Carbon*, 2019, **152**, 434.
163 S. Sun, J. Chen, K. Jiang, Z. Tang, Y. Wang, Z. Li, C. Liu, A. Wu and H. Lin, *ACS Appl. Mater. Interfaces*, 2019, **11**, 5791.
164 H. Zhao, A. Vomiero and F. Rosei, *Small*, 2020, **16**, 2000804.
165 R. R. Zairov, K. A. Sarkanich, I. R. Nizameev, A. V. Luzhetskiy, S. N. Sudakova, S. N. Podyachev, V. A. Burilov, I. M. Vatsouro, A. Vomiero and A. R. Mustafina, *Nanomater*, 2021, **11**, 3080.
166 Y. Xu, Y. Yang, S. Lin and L. Xiao, *Anal. Chem.*, 2020, **92**, 15632.
167 C. Wang, K. Jiang, Q. Wu, J. Wu and C. Zhang, *Chem. – Eur. J.*, 2016, **22**, 14475.
168 A. Zhu, Q. Qu, X. Shao, B. Kong and Y. Tian, *Angew. Chem., Int. Ed.*, 2012, **51**, 7185.
169 C. Wang, T. Hu, T. Thomas, S. Song, Z. Wen, C. Wang, Q. Song and M. Yang, *Nanoscale*, 2018, **10**, 21809.
170 X. W. Hua, Y. W. Bao, J. Zeng and F. G. Wu, *ACS Appl. Mater. Interfaces*, 2019, **11**, 32647.
171 Y. Li, G. Bai, S. Zeng and J. Hao, *ACS Appl. Mater. Interfaces*, 2019, **11**, 4737.
172 H. Zhang, G. Wang, Z. Zhang, J. H. Lei, T. M. Liu, G. H. Xing, C. X. Deng, Z. Tang and S. Qu, *Light: Sci. Appl.*, 2022, **11**, 113.
173 R. Mazzaro and A. Vomiero, *Adv. Energy Mater.*, 2018, **8**, 1801903.
174 Y. Zhou, D. Benetti, Z. Fan, H. Zhao, D. Ma, A. O. Govorov, A. Vomiero and F. Rosei, *Adv. Energy Mater.*, 2016, **6**, 1501913.
175 K. B. Cai, H. Y. Huang, M. L. Hsieh, P. Chen, S. Chiang, S. H. Chang, J. L. Shen, W. R. Liu and C. T. Yuan, *ACS Nano*, 2022, **16**(3), 3994.
176 J. Wang, L. Tang, G. Zeng, Y. Deng, H. Dong, Y. Liu, L. Wang, B. Peng, C. Zhang and F. Chen, *Appl. Catal., B*, 2018, **222**, 115.
177 M. C. Ortega-Liebana, J. L. Hueso, S. Ferdousi, K. L. Yeung and J. Santamaria, *Diamond Relat. Mater.*, 2016, **65**, 176.
178 P. Roy, P. C. Chen, A. P. Periasamy, Y. N. Chen and H. T. Chang, *Mater. Today*, 2015, **18**, 447.
179 T. Gao, X. Wang, L.-Y. Yang, H. He, X. X. Ba, J. Zhao, F. L. Jiang and Y. Liu, *ACS Appl. Mater. Interfaces*, 2017, **9**, 24846.
180 X. Hu, H. Zhao, Y. Liang, F. Chen, J. Li and R. Chen, *Chemosphere*, 2021, **264**, 128434.